Atmos. Chem. Phys., 26, 3467–3487, 2026
https://doi.org/10.5194/acp-26-3467-2026

Atmospheric Chemistry and Physics
Open Access
EGU

Measurement report: Three-year characteristics of sulfuric acid in urban Beijing and derivation of daytime sulfuric acid proxies applicable to inland sites

Yishuo Guo[1,2], Chao Yan[2,3], Chang Li[2], Chenjuan Deng[4], Ying Zhang[2,3], Ying Zhou[2], Haotian Zheng[4], Yueqi Jiang[4], Xin Chen[2], Wei Ma[2], Nina Sarnela[5], Zhuohui Lin[2], Chenjie Hua[2], Xiaolong Fan[6], Feixue Zheng[2], Zemin Feng[2], Zongcheng Wang[2], Yusheng Zhang[2], Jingkun Jiang[4], Bin Zhao[4], Markku Kulmala[2,3,5], and Yongchun Liu[2]

[1]College of Environmental and Chemical Engineering, Hebei Vocational University of Industry and Technology, Shijiazhuang, Hebei, China
[2]Aerosol and Haze Laboratory, Beijing Advanced Innovation Center for Soft Matter Science and Engineering, Beijing University of Chemical Technology, Beijing, China
[3]Nanjing-Helsinki Institute in Atmospheric and Earth System Sciences, Nanjing University, Suzhou, China
[4]State Key Joint Laboratory of Environment Simulation and Pollution Control, State Environmental Protection Key Laboratory of Sources and Control of Air Pollution Complex, School of Environment, Tsinghua University, Beijing 100084, China
[5]Institute for Atmospheric and Earth System Research/Physics, Faculty of Science, University of Helsinki, Helsinki, Finland
[6]Center for Excellence in Regional Atmospheric Environment, Key Lab of Urban Environment and Health, Institute of Urban Environment, Chinese Academy of Sciences, Xiamen, China

Correspondence: Chao Yan (chaoyan@nju.edu.cn) and Yongchun Liu (liuyc@buct.edu.cn)

Received: 3 September 2025 – Discussion started: 29 September 2025
Revised: 19 February 2026 – Accepted: 20 February 2026 – Published: 6 March 2026

Abstract. Sulfuric acid (H_2SO_4) is a key precursor in atmospheric new particle formation and cluster early growth. However, long-term measurement of it is only available at a few sites. Although several proxies for estimating H_2SO_4 concentration have been proposed, they are always site-specific. Therefore, both reliable H_2SO_4 measurement and proxies with wider application are highly needed. Here, we conducted a long-term H_2SO_4 measurement in urban Beijing during 2019–2021, and derived three H_2SO_4 proxies based entirely on its formation and loss pathways. Results show that daytime H_2SO_4 concentration is 2.0–7.4 $\times 10^6$ molec. cm^{-3} and shows an overall decline with an average annual decrease of 14 %. This decline is mainly due to the ongoing SO_2 emission controls. Daytime H_2SO_4 shows a clear seasonal variation that tracks UVB. Nighttime H_2SO_4 concentration is 1.6–6.3 $\times 10^5$ molec. cm^{-3}, with higher levels in warmer seasons due to stronger sources and lower condensation sink (CS). The diurnal variations of H_2SO_4 across seasons follow those of photo-oxidation-related parameters, such as UVB, OH radical, and photolysis rate of NO_2 ($J(NO_2)$). All of the three proxies can reproduce H_2SO_4 concentration during 10:00–14:00 LT. Importantly, they can estimate H_2SO_4 concentration at a boreal forest site in Hyytiälä, Finland, suggesting their applicability to sites with diverse environments. Furthermore, the parameters used in UVB-$PM_{2.5}$ based proxy are available at most observational sites. Further application of this proxy could provide H_2SO_4 concentrations covering many regions worldwide, which may further facilitate research on atmospheric nucleation and secondary aerosol growth of these sites.

Published by Copernicus Publications on behalf of the European Geosciences Union.

1 Introduction

New particle formation (NPF) is a key contributor to the born of atmospheric aerosols (Merikanto et al., 2009; Gordon et al., 2017), and thus can have a great influence on global climate and human health (Hartmann et al., 2014; Lelieveld et al., 2015). Among all the precursors that drive atmospheric nucleation, the initial step of NPF, sulfuric acid (H_2SO_4) has been shown to be the most important one from both laboratory experiments and field observations (Kulmala et al., 2006; Riipinen et al., 2007; Paasonen et al., 2009; Erupe et al., 2010; Wang et al., 2011; Kirkby et al., 2011; Yu et al., 2012; Almeida et al., 2013; Kürten et al., 2014; Riccobono et al., 2014; Lehtipalo et al., 2018; Yao et al., 2018; Lee et al., 2019; Myllys et al., 2019; Yan et al., 2021). The clusters formed by sulfuric acid and base molecules, such as ammonia and amines, provide the primary core for further condensation of other low-volatility species, promoting aerosols growth to tens of nanometers, reaching the sizes of cloud condensation nuclei (CNN) and ultrafine particles. Therefore, reliable measurement of sulfuric acid is of great importance.

Since the 1990s, sulfuric acid measurements have been conducted in various field campaigns that covered a wide range of atmospheric environments, including urban (McMurry et al., 2005; Fiedler et al., 2005; Riipinen et al., 2007; Mikkonen et al., 2011; Wang et al., 2011; Yao et al., 2018; Lu et al., 2019), rural (Berresheim et al., 2000; Birmili et al., 2003; Paasonen et al., 2009; Erupe et al., 2010; Mikkonen et al., 2011; Kürten et al., 2016; Yang et al., 2021a, 2023), mountainous (Weber et al., 1996, 1997; Boy et al., 2008; Mikkonen et al., 2011), marine (Berresheim et al., 1993, 2002; Weber et al., 1995, 1996; O'Dowd et al., 2002), forest environments (Fiedler et al., 2005; Riipinen et al., 2007; Petäjä et al., 2009; Nieminen et al., 2009; Mikkonen et al., 2011; Jokinen et al., 2012), among others (Weber et al., 1998; Mauldin et al., 2001, 2004; Sarnela et al., 2015; Jokinen et al., 2018). The locations of these sites, measurement periods, and corresponding sulfuric acid concentrations are summarized in Table 1. In general, within the planetary boundary layer, sulfuric acid concentration was around 0.2–15×10^6 cm^{-3}, with the highest levels in urban areas, followed by rural, mountainous, and marine regions, and the lowest in forest areas. This suggests that sulfuric acid levels depend strongly on the intensity of human activity. In addition, most measurement campaigns lasted for less than four months and concentrated mostly on warmer seasons (spring, summer and early autumn) when NPF usually occurs (Dal Maso et al., 2005; Manninen et al., 2009; Dada et al., 2017; Nieminen et al., 2018; Chu et al., 2019; Qi et al., 2015). Previous studies showed that NPF in Chinese megacities was also frequently observed in winter (Deng et al., 2020; Chu et al., 2019), and thus sulfuric acid measurement in cold seasons is also crucial. To date, however, long-term measurement of sulfuric acid worldwide is still lacking, which somewhat limits the investigation of NPF processes.

To complement the limited sulfuric acid measurement, several sulfuric acid proxies were developed. The original expression for estimating sulfuric acid concentration was derived from its production and loss pathways. Assuming that sulfuric acid originates solely from OH-initiated oxidation of SO_2 and the only loss is the condensation sink (CS) onto particle surfaces, the steady-state concentration of sulfuric acid can be expressed as $[H_2SO_4] = k \cdot [OH][SO_2]/CS$, where k is the rate constant of $OH + SO_2$ reaction. As early as 1997, Weber et al. (1997) estimated sulfuric acid concentrations at a marine site and a mountain site using this expression (Weber et al., 1997). Results showed that the estimated daytime sulfuric acid for two selected days generally matched the measured one at both sites. Later, Berresheim et al. (2002) also utilized this expression at a coastal site (Berresheim et al., 2002). However, when the accommodation coefficient of CS calculation was chosen as 1, the estimated sulfuric acid concentration turned out to be much lower than the measured one. The authors speculated that additional sulfuric acid sources might exist, likely the OH- or BrO-initiated oxidation of dimethyl disulfide or dimethyl sulfide, or the oxidation of SO_2 by non-OH oxidants. This also suggests that this proxy may not be suitable for coastal environments. In 2009, Petäjä et al. (2009) proposed the concept of sulfuric acid proxy clearly and derived three proxies based on its source-sink equilibrium (Petäjä et al., 2009). The first proxy, $P_1 = k_1 \cdot [OH][SO_2]/CS$, was very similar to that proposed by Weber et al., but the pre-factor k_1 was obtained by the fitting of measurement data. During daytime, OH radical mainly arises from photochemical reactions. Therefore, OH radical in P_1 could be replaced by UVB, yielding the second proxy of $P_2 = k_2 \cdot [UVB][SO_2]/CS$. Similarly, replacing OH radical with global radiation yielded the third proxy, $P_3 = k_3 \cdot [Glob][SO_2]/CS$. These three proxies showed good performance in estimating daytime sulfuric acid concentration. However, the authors noted that k_1, k_2 and k_3 came from fits so that they are likely site-specific, which limits their transferability to other sites.

Later, Mikkonen et al. (2011) attempted to develop sulfuric acid proxies suitable for various environments. The datasets came from five sites, including one forest, one mountainous, two rural and one urban sites (Mikkonen et al., 2011). Five linear-fitting proxies, including one (Eq. 1) similar to the P_3 proxy proposed by Petäjä et al. (2009), were first built.

$$L1 = B \cdot k \cdot \text{Radiation} \cdot [SO_2] \cdot CS^{-1} \quad (1)$$

Results showed only minor differences among the five proxies, with L3 proxy (Eq. 2) generally performing the best.

$$L3 = B \cdot k \cdot \text{Radiation} \cdot [SO_2]^{0.5} \quad (2)$$

Based on this, the authors concluded that the pseudo-steady-state assumption for gaseous sulfuric acid could be somewhat

Table 1. Summary of atmospheric sites with sulfuric acid measurement.

Type of site	Location	Measurement period	H_2SO_4 ($\times 10^6$ molec. cm^{-3})	References
Urban	Atlanta, Georgia, USA	Aug 2002	2.9	McMurry et al. (2005) Mikkonen et al. (2011)
	Heidelberg, Germany	Mar–Apr 2004	3.0	Fiedler et al. (2005) Riipinen et al. (2007)
	Beijing, China	Jul–Sep 2008	1.0–9.0	Wang et al. (2011)
	Shanghai, China	Mar 2014–Feb 2016	7.8	Yao et al. (2018)
	Beijing, China	Feb–Mar 2018	4.9	Lu et al. (2019)
Rural	Hohenpeissenberg, Germany	151 d in 1998 186 d in 1999	0.1–10	Berresheim et al. (2000)
		Apr 1998–Jul 2000	0.6	Birmili et al. (2003) Paasonen et al. (2009) Mikkonen et al. (2011)
	Ohio, USA	Aug 2008–Nov 2009	winter: 0.6 spring: 5.2 summer: 2.9 autumn: 0.5	Erupe et al. (2010)
	San Pietro Capofiume, Italy	Jun–Jul 2009	2.4	Mikkonen et al. (2011)
	Melpitz, Germany	May 2008	2.9	Mikkonen et al. (2011)
	Vielbrunn, Germany	May–Jun 2014	3.0	Kürten et al. (2016)
	Nanjing, China	Dec 2017–Jan 2018 Apr 2018 Jul–Aug 2018 Nov 2018	winter: 1.9 spring: 7.4 summer: 4.5 autumn: 9.0	Yang et al. (2021a)
	Xiamen, China	Jul–Aug 2022	2.3	Yang et al. (2023)
Mountain	Colorado, USA	Sep 1993	0.1–10	Weber et al. (1996, 1997)
		Jun–Jul 2006	2.8	Boy et al. (2008)
		Jun–Jul 2007	1.4	Mikkonen et al. (2011)
Marine	Washington, USA	Apr 1991	0.03–32.0	Berresheim et al. (1993)
	Hawaii, USA	Jul 1992	upslope: 1.2 downslope: 0.5	Weber et al. (1995) Weber et al. (1996)
	Mace Head, Ireland	Jun 1999	1.5	Berresheim et al. (2002)
		Sep 1998 Jun 1999	2.0–15.0	O'Dowd et al. (2002)
Forest	Hyytiälä, Finland	Mar–Apr 2003	2.6	Fiedler et al. (2005)
		Apr–May 2005	1.0–10	Riipinen et al. (2007)
		Mar–Jun 2007	0.9–2.5	Petäjä et al. (2009) Nieminen et al. (2009)
		Mar–Apr 2003	0.6	Mikkonen et al. (2011)
		Mar–Jun 2007	0.2	Mikkonen et al. (2011)
		Mar–Apr 2011	0.3–10	Jokinen et al. (2012)
Others	Macquarie Island, Australia	27 Nov 1995	2.8	Weber et al. (1998)
	Antarctica	Dec 1998	0.3	Mauldin et al. (2001)
		Nov–Dec 2000	0.3	Mauldin et al. (2004)
		Nov 2014–Jan 2015	0.2–10	Jokinen et al. (2018)
	Kilpilahti, Finland	Jun–Jul 2012	oil refinery: 11.5 industrial: 4.4 non-industrial: 1.3	Sarnela et al. (2015)

unrealistic in atmospheric conditions, and then proposed five additional nonlinear-fitting sulfuric acid proxies. However, only correlation coefficients were used to evaluate the performance of five linear fitting proxies, and these correlation coefficients were close to each other. Thus, the above conclusion requires more data to be supported.

Based on these studies, Lu et al. (2019) developed seven nonlinear-fitting proxies to estimate daytime sulfuric acid concentration in urban Beijing (Lu et al., 2019). In proxies of N5–N7, O_3 and HONO were included to account for OH radical formation via photolysis of HONO. Results showed that seven proxies generally performed well in estimating daytime sulfuric acid concentration with similar correlation coefficients and relative errors. Nevertheless, the authors concluded that N7 proxy (Eq. 3) was the most suitable for estimating daytime sulfuric acid, as it took the CS oss pathway into account, had the lowest relative error and used the easily measured NO_x.

$$[H_2SO_4] = 0.0013\mathrm{UVB}^{0.13} \cdot [SO_2]^{0.40} \cdot \mathrm{CS}^{-0.17} \cdot [O_3]^{0.44} + [NO_x]^{0.41} \quad (3)$$

Note that this proxy was developed for urban Beijing, and thus may not apply to other sites. A year later, Dada et al. constructed proxies based on the source-sink equilibrium of sulfuric acid at four different sites, including one boreal forest, one rural, one urban, and one megacity sites. The formation of sulfuric acid from the ozonolysis of alkenes was first considered. Results showed that P_1 (Eq. 4) and P_3 (Eq. 5) proxies with the alkene ozonolysis term could estimate both daytime and nighttime sulfuric acid well, while P_2 proxy (Eq. 6) without the alkene ozonolysis term could only estimate daytime sulfuric acid.

$$\left([H_2SO_4] = \frac{\mathrm{CS}}{2k_3} + \sqrt{\left(\frac{\mathrm{CS}}{2k_3}\right)^2 + \frac{[SO_2]}{k_3}(k_1 \cdot \mathrm{GlobRad} + k_2 \cdot [O_3][\mathrm{Alkenes}])}\right) \quad (4)$$

$$[H_2SO_4] = \frac{k_1 \cdot \mathrm{GlobRad}[SO_2] + k_2 \cdot [SO_2][O_3][\mathrm{Alkene}]}{\mathrm{CS}} \quad (5)$$

$$[H_2SO_4] = \frac{\mathrm{CS}}{2k_3} + \sqrt{\left(\frac{\mathrm{CS}}{2k_3}\right)^2 + \frac{[SO_2]}{k_3}k_1 \cdot \mathrm{GlobRad}} \quad (6)$$

Although the proxy equations were the same across sites, the parameters therein were different. Thus, these four proxies have limited application at other sites.

In this study, we characterize the interannual, seasonal, and diurnal variations of sulfuric acid in urban Beijing and derive proxies to estimate sulfuric acid concentration at various sites. Long-term measurement of sulfuric acid covering nearly three continuous years (from 1 January 2019 to 11 November 2021) was conducted in urban Beijing. First, the yearly and seasonal variation of sulfuric acid concentration, as well as its diurnal cycles were analyzed. Second, the performance of nine representative proxies, including seven steady-state based ones and two numerical regression ones, from previous studies at our site was investigated. Based on these analyses, three steady-state proxies were proposed according to the budget analysis of sulfuric acid, and their performance and limitations on estimating daytime sulfuric acid concentration were investigated in detail. These three proxies were then applied to estimate sulfuric acid concentration at a boreal forest site in Hyytiälä, Finland. Correlation coefficients and relative errors indicate that three proxies are able to reproduce daytime sulfuric acid well, suggesting that three proxies and parameters therein could be applicable at other atmospheric sites. Finally, a general suggestion on proxy selection with different available parameters was given.

2 Method

2.1 Measurement site

The measurements were conducted at the Aerosol and Haze Laboratory at the west campus of Beijing University of Chemical Technology (39.95° N, 116.31° E). It is a typical urban site surrounded by commercial and residential areas and three major roads (Liu et al., 2020; Yan et al., 2021, 2022; Guo et al., 2021). The datasets used in this study span nearly three continuous years from January 2019 to November 2022.

2.2 Measurement of sulfuric acid

Sulfuric acid was measured by a long time-of-flight chemical ionization mass specter (LTOF-CIMS, Aerodyne Research, Inc.) using nitric acid as reagent ions. The basic working principle of this instrument is described elsewhere (Jokinen et al., 2012), and the instrument configuration has been provided in our previous studies and has remained unchanged over the years. Briefly, air was drawn through a stainless-steel tube (1.6 m long, 3/4 inch in diameter). The inlet flow rate was maintained at 7.2 L min^{-1}. Additionally, a flush plate (Karsa Inc.) was installed to effectively remove water vapor in the sampled air.

Sulfuric acid concentration was quantified from the ratio of bisulfate ions (with counting rates unit in ions per second) to primary ions as follows:

$$H_2SO_4 = \frac{HSO_4^- + H_2SO_4NO_3^-}{NO_3^- + HNO_3NO_3^- + (HNO_3)_2NO_3^-} \times C \quad (7)$$

where C is the calibration coefficient, determined by direct calibration using known amounts of gaseous sulfuric acid injected into the instrument (Kürten et al., 2012). During the measurement period, the instrument ran stably. Calibration was performed every six months and after tuning. After correcting the diffusional wall loss of the sampling line (0.2129), the final calibration coefficients were 6.07–7.47 $\times 10^9$ molec. cm^{-3} over the 3-year period.

2.3 Other ancillary measurements

Particle number concentration and size distribution was measured by a differential mobility particle sizer (DMPS, 6–840 nm) (Aalto et al., 2001) and a particle size distribution system (PSD, 3 nm–10 µm) (Liu et al., 2016). The configuration of these two instruments have been described in our previous studies (Zhou et al., 2021; Yan et al., 2021). Based on these measurements, the condensation sink (CS) of sulfuric acid can be calculated from the following Eq. (2) (Kulmala et al., 2012):

$$\mathrm{CS} = 4\pi D \int_0^{d_{\mathrm{p}}\max} \beta_m \left(d'_{\mathrm{p}}\right) d'_{\mathrm{p}} N'_{\mathrm{d_p}} d d'_{\mathrm{p}} = 4\pi D \sum_{d'_{\mathrm{p}}} \beta_{m,d'_{\mathrm{p}}} d'_{\mathrm{p}} N_{\mathrm{d'_p}} \quad (8)$$

where D is the diffusion coefficient of sulfuric acid, d'_{p} is the particle diameter, $N_{\mathrm{d'_p}}$ is the particle number concentration with diameter d'_{p}, and β_m represents the transition-regime correction. Size-resolved hygroscopic growth of aerosols was considered in the calculation of CS. CS values calculated from two instruments are shown in Fig. S13. The datasets from PSD was chosen in priority as it measures wider size ranges. If PSD data was unavailable or not consecutive for more than 10–20 d, DMPS data was used. There were three periods during which measurements from both instruments were continuous and stable, and the CS comparison for these periods are shown in Fig. S14. Compared with PSD CS values, DMPS CS values were on average ∼ 11.7 % lower.

Meteorological parameters were measured by a weather station (AWS310, Vaisala Inc.) located on the building rooftop. These parameters include ambient temperature, relative humidity (RH), pressure, visibility, UVB radiation, and horizontal wind speed and direction. Trace gases, including carbon monoxide (CO), sulfur dioxide (SO_2), nitrogen oxides (NO_x), and ozone (O_3), were monitored using four Thermo Environmental Instruments (models 48i, 43i-TLE, 42i, 49i, respectively). Calibrations of these instruments were performed every two weeks using standard gases of known concentrations. The mass concentration of $PM_{2.5}$ and PM_{10} were measured with a tapered element oscillating microbalance dichotomous ambient particulate monitor (TEOM 1405-DF, Thermo Fisher Scientific Inc., USA). The mass concentration of PM_{coarse} was obtained based on the difference between PM_{10} and $PM_{2.5}$.

2.4 Modelling of OH radical, J(NO_2) and J(O^1D)

The Weather Research and Forecasting Model-Community Multiscale Air Quality (WRF-CMAQ) model was applied to simulate the concentration of OH radical, the photolysis rate of NO_2 (J(NO_2)) and the photolysis rate for producing excited atomic oxygen from O_3 (J(O^1D)). Simulations covered the period from 1 January 2019 to 19 February 2020. The physical options in WRF (version 3.9.1) were the same as in Zheng et al. (2019a). The CMAQ model (version 5.3.2) was coupled with the two-dimensional Volatility Basis Set (2D-VBS) (Zhao et al., 2016), where the SAPRC07 mechanism was adopted for gas-phase chemistry, and the AERO6 (Sarwar et al., 2011) was used for aerosol module. The modelling domain was the same as in Zheng et al. (2020), where the horizontal resolution was 27 km × 27 km and the vertical grid had 14 layers. Default planetary boundary layer settings were used. To minimize the influence of initial conditions, simulations were spun up 5 d before the modelling period. This WRF-CMAQ model and the emission inventory have been widely applied and validated in previous studies using multiple lines of evidence, including ground-based monitoring networks and satellite retrievals ...(Zhao et al., 2018; Zheng et al., 2019a, b, 2023, 2024; Chang et al., 2023). Simulated concentrations of key pollutants agree well with observations in both magnitude and temporal variability (Tables S5–S7). These demonstrate that the modeling system reasonably reproduces the spatial and temporal variations of major air pollutants across China.

3 Results and discussion

3.1 Characteristics of measured sulfuric acid

3.1.1 Interannual and monthly variations of sulfuric acid

In the early morning, sulfuric acid concentration is influenced not only by the photochemical production and loss pathways, but also by additional sources, such as SO_2 oxidation on traffic-related black carbon (Yao et al., 2020). In addition, sulfuric acid from direct emission and the ozonolysis of alkenes cannot be ignored during daytime when far from noon (Yang et al., 2021a). Therefore, daytime window of 10:00–14:00 LT (local time) was chosen for proxy evaluation unless specified otherwise. This period also corresponds to the new particle formation time (Kulmala et al., 2007, 2013; Deng et al., 2020; Ma et al., 2021). The corresponding nighttime window was 22:00–02:00 LT next day.

In urban Beijing, typical daytime sulfuric acid concentration ranges from 2.0×10^6 to 7.4×10^6 molec. cm^{-3} (monthly median concentration, Fig. 1a and Table 2). Figures 1a and S1e in the Supplement show that sulfuric acid concentration generally declines from 2019 to 2021, with an average annual decrease of 14 %. During the three years, UVB intensity remains roughly constant (Figs. 1b and S1a), CS change is not significant (Figs. 1d and S1e), while SO_2 concentration decreases markedly (Figs. 1c and S1d). Thus, the yearly decline of sulfuric acid is mainly attributed to the decrease of SO_2 (by ∼ 25 % yr^{-1}, Table S8). Figure 1a also reveals that sulfuric acid concentration has a clear seasonal variation, which is the highest in May ($4.2–7.4\times10^6$ molec. cm^{-3}) and September ($5.0–7.2\times10^6$ molec. cm^{-3}) and the lowest from November to February of the next year ($2.0–3.3\times10^6$ molec. cm^{-3}). UVB shows the same monthly pattern as sulfuric acid, which reaches the highest from May to Septem-

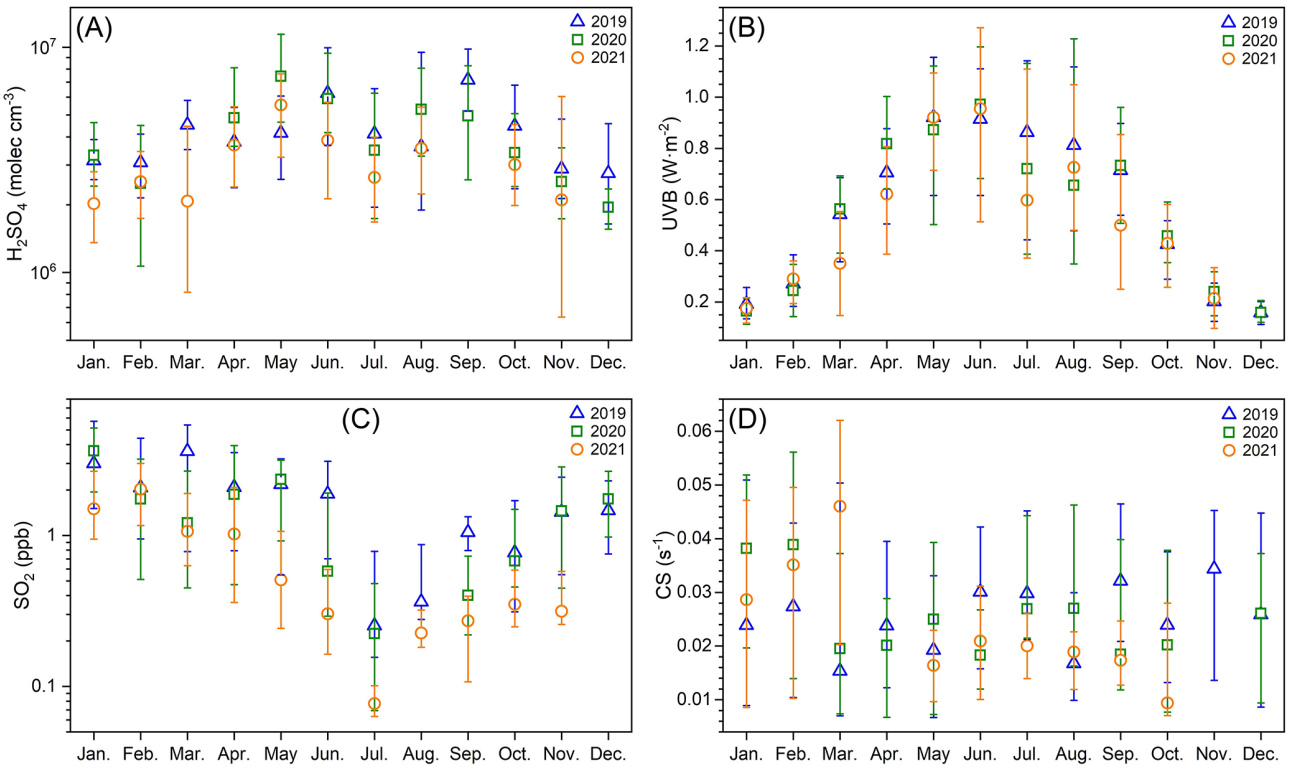

Figure 1. Three-year (from January 2019 to November 2021) monthly variations of **(a)** H_2SO_4 concentration, **(b)** UVB, **(c)** SO_2 and **(d)** condensation sink (CS) during daytime (10:00–14:00 LT) when new particle formation mostly occurs. Blue triangles, green squares and orange circles represent data in 2019, 2020 and 2021, respectively. The up line, middle marker and bottom line stand for upper quartile, median and lower quartile values, respectively.

Table 2. Monthly concentration of H_2SO_4 (molec. cm^{-3}) during daytime (10:00–14:00 LT) from 2019 to 2021. "NaN" means there is no data available. Bold values denote the highest or lowest monthly median concentrations.

Month	2019			2020			2021		
	Median	25th	75th	Median	25th	75th	Median	25th	75th
January	3.1×10^6	2.6×10^6	3.9×10^6	3.3×10^6	2.4×10^6	4.6×10^6	$\mathbf{2.0 \times 10^6}$	1.4×10^6	2.8×10^6
February	3.1×10^6	2.1×10^6	4.1×10^6	2.5×10^6	1.1×10^6	4.5×10^6	2.5×10^6	1.7×10^6	3.4×10^6
March	4.5×10^6	3.5×10^6	5.8×10^6	NaN	NaN	NaN	2.1×10^6	8.2×10^5	4.5×10^6
April	3.8×10^6	2.4×10^6	5.4×10^6	4.9×10^6	3.6×10^6	8.1×10^6	3.7×10^6	2.4×10^6	5.4×10^6
May	4.2×10^6	2.6×10^6	6.1×10^6	$\mathbf{7.4 \times 10^6}$	4.7×10^6	1.1×10^7	5.5×10^6	3.3×10^6	7.6×10^6
June	6.2×10^6	3.7×10^6	1.0×10^7	5.9×10^6	4.2×10^6	9.4×10^6	3.9×10^6	2.1×10^6	5.7×10^6
July	4.1×10^6	2.0×10^6	6.6×10^6	3.5×10^6	1.7×10^6	6.3×10^6	2.6×10^6	1.7×10^6	4.0×10^6
August	3.6×10^6	1.9×10^6	9.5×10^6	5.3×10^6	3.3×10^6	8.1×10^6	3.6×10^6	2.2×10^6	5.4×10^6
September	7.2×10^6	5.2×10^6	9.8×10^6	5.0×10^6	2.6×10^6	8.3×10^6	NaN	NaN	NaN
October	4.5×10^6	2.4×10^6	6.8×10^6	3.4×10^6	2.4×10^6	5.1×10^6	3.0×10^6	2.0×10^6	4.5×10^6
November	2.9×10^6	2.1×10^6	4.8×10^6	2.5×10^6	1.7×10^6	3.6×10^6	2.1×10^6	6.3×10^5	6.0×10^6
December	2.8×10^6	1.6×10^6	4.6×10^6	$\mathbf{2.0 \times 10^6}$	1.6×10^6	2.4×10^6	NaN	NaN	NaN

ber and decreases to the lowest from November to February of next year, while SO_2 shows an opposite monthly trend to sulfuric acid. This indicates that the influence of UVB on sulfuric acid monthly variation outperforms that of SO_2. Meanwhile, sulfuric acid concentration in July is much lower from May to September, likely driven by extremely low SO_2 despite a small decrease of UVB in that month. In Beijing, precipitation occurs more frequently in July and August than in May, June and September (Table S1 in the Supplement). This reduces UVB and SO_2 in these two months (Fig. S2), and fur-

ther leads to lower sulfuric acid concentration. Overall, UVB intensity and SO_2 concentration are the two key parameters determining sulfuric acid concentration.

Typical nighttime sulfuric acid concentration of urban Beijing ranges from 1.6×10^5 to 6.3×10^5 molec. cm^{-3} (monthly median concentration, Fig. S3 and Table S2), about one order of magnitude lower than that of daytime. Unlike daytime sulfuric acid, nighttime sulfuric acid concentration does not show a decreasing trend from 2019 to 2021. At night, under clean conditions, alkene ozonolysis is a major source of sulfuric acid (Guo et al., 2021); under more polluted conditions, primary emissions from vehicles or fresh plumes indicated by benzene also play an important role (Yang et al., 2021a). However, data of alkenes and benzene is unavailable in July–August 2019 and in 2020–2021, making it impossible to estimate the intensities of these nocturnal sulfuric acid sources. Thus, we are not able to give further explanation on the yearly variation of nighttime sulfuric acid. Figure S3a shows that nighttime sulfuric acid has a similar but weaker seasonal variation as that of daytime, i.e., concentration is generally higher from May to September than in other months, and concentration in July and August is significantly lower than in May, June and September. According to the data of 2019, the direct-emission source is higher from March to June (Fig. S3b), and alkene-ozonolysis source is higher from March to September (Fig. S3c), indicating that the sources of nighttime sulfuric acid are stronger in warmer seasons. Meanwhile, the CS level is lower from April to October (Fig. S3d), resulting in lower losses of sulfuric acid. Together, these two factors lead to higher nighttime sulfuric acid concentrations during warmer seasons.

3.1.2 Diurnal variations of sulfuric acid and related parameters

The diurnal patterns of sulfuric acid across seasons are similar, starting increasing in the early morning (~ 04:00–06:00 LT), peaking around noon (~ 11:00 LT), and decreasing to a low level at nightfall (~ 19:00 LT) (Fig. 2a). The morning increase of sulfuric acid occurs earliest in summer, followed by spring, autumn and winter. Moreover, the peak width of sulfuric acid from the widest to narrowest follows the same seasonal trend. These diurnal patterns across the four seasons resemble those of UVB (Fig. 2b), suggesting that radiation-driven photochemical reactions govern sulfuric acid formation. Moreover, the morning increase of sulfuric acid occurs earlier than UVB and global radiation but close to $J(NO_2)$ and OH radical (Fig. S4d). This suggests that UVB and global radiation are not able to adequately represent the photochemical sources in early morning, whereas SO_2 oxidation by OH radical produced by NO_2 photolysis is a major source. HONO photolysis is another major formation pathway for OH radical (Tan et al., 2017, 2018; Ma et al., 2019, 2022; Yang et al., 2021b). HONO decreases in the morning at ~ 06:00–07:00 LT, more than an hour after the morning increase of sulfuric acid and OH radical (Fig. S4d). This suggests that sulfuric acid formation in the early morning is not likely caused by the oxidation of OH radical from HONO photolysis. The daytime peaking hour of sulfuric acid is close to $J(NO_2)$ and $J(O^1D)$ (Fig. S4b), indicating that sulfuric acid peaking hour is controlled by photochemical reactions related to $J(NO_2)$ and $J(O^1D)$. The peak width of sulfuric acid is the widest, followed by $J(NO_2)$, global radiation, OH radical, $J(O^1D)$ and UVB (Fig. S4c). This implies that when using proxies with these parameters to estimate daytime sulfuric acid concentration, differences in peaking hours and peak widths may cause deviations from the measured concentration.

During the day, sulfuric acid concentration is the highest in summer, followed by spring and autumn, and then winter. This seasonal variation generally tracks UVB, except in autumn, when UVB and SO_2 are lower than spring, but daytime sulfuric acid concentration remains comparable to that in spring. In autumn, the frequency of sulfuric acid with high concentrations ($\geq 1.2\times10^7$ molec. cm^{-3}) is higher than spring (Fig. S5), likely contributing to the overall higher level of sulfuric acid. At night, sulfuric acid concentrations are comparable across seasons, even though SO_2 and CS levels vary. As aforementioned, additional sources such as benzene-related emissions (Yang et al., 2021a) are among the main nighttime sources of sulfuric acid, so nighttime sulfuric acid cannot be easily interpreted by proxies only including SO_2, CS and OH radical.

3.2 Performance of sulfuric acid proxies from previous study

In previous studies, several representative proxies for sulfuric acid that incorporate real physical and chemical considerations have been proposed. Before constructing the proxy for this study, we first evaluate the performance of existing proxies on estimating sulfuric acid concentration. The equations and internal parameters of these nine proxies are listed in Table 3 (Petäjä et al., 2009; Mikkonen et al., 2011; Lu et al., 2019; Dada et al., 2020). Figure 3 shows the measured sulfuric acid concentration and the proxy-estimated concentrations during daytime (10:00–14:00 LT) in 2019. Table S3 summarizes the corresponding mean, standard deviation, median, lower quartile and upper quartile of sulfuric acid concentrations. To have a more accurate understanding on proxy performance, the correlation coefficients, power exponents, and slopes of the linear fittings between measured and estimated sulfuric acid, as well as the relative errors of estimated to measured sulfuric acid concentrations are further evaluated (Table 4). The relative error is calculated as follows (Lu et al., 2019):

$$\mathrm{RE} = \frac{1}{n}\cdot\sum_{i=1}^{n}\frac{|[H_2SO_4]_{\mathrm{pro},i} - [H_2SO_4]_{\mathrm{mea},i}|}{[H_2SO_4]_{\mathrm{mea},i}}. \quad (9)$$

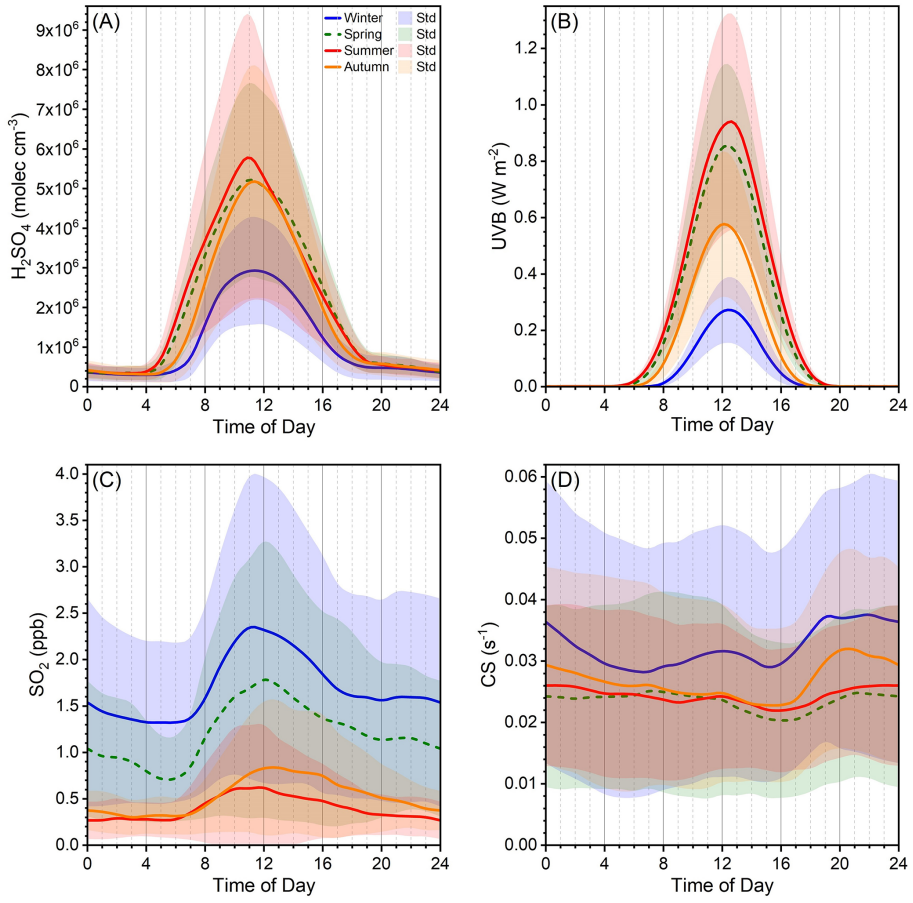

Figure 2. Three-year (from 2019 to 2021) diurnal variations of **(a)** H_2SO_4, **(b)** UVB, **(c)** SO_2 and **(d)** condensation sink (CS). Winter, spring, summer and autumn periods cover 15 November to 15 March of next year, 16 March to May, June to August, and September to 14 November, respectively. Lines are the mean values, and shaded areas denote the standard deviations of the data.

Table 3. The equations and internal parameters of nine sulfuric acid proxies from literatures.

Proxy	Equation	Parameters	Reference
$\text{Proxy}_{\text{Petäjä OH–C}}$ $\text{Proxy}_{\text{Petäjä OH–F}}$	$P_1 = \frac{k_1 \cdot [SO_2] \cdot [OH]}{CS}$	$k_1 = 2.2 \times 10^{-12}$ cm^3 molec.$^{-1}$ s^{-1} $k_1 = 8.6 \times 10^{-10} \times [OH]^{-0.48}$ cm^3 s^{-1}	Petäjä et al. (2009)
$\text{Proxy}_{\text{Petäjä UVB–C}}$ $\text{Proxy}_{\text{Petäjä UVB–F}}$	$P_2 = \frac{k_2 \cdot [SO_2] \cdot UVB}{CS}$	$k_2 = 9.9 \times 10^{-7}$ m^2 W^{-1} s^{-1} $k_2 = 8.4 \times 10^{-7} \times UVB^{-0.68}$ m^2 W^{-1} s^{-1}	
$\text{Proxy}_{\text{Petäjä Glob–C}}$ $\text{Proxy}_{\text{Petäjä Glob–F}}$	$P_3 = \frac{k_3 \cdot [SO_2] \cdot Glob}{CS}$	$k_3 = 2.3 \times 10^{-9}$ m^2 W^{-1} s^{-1} $k_3 = 1.4 \times 10^{-7} \times Glob^{-0.70}$ m^2 W^{-1} s^{-1}	
$\text{Proxy}_{\text{Mikkonen et al.}}$	$a \cdot k \cdot \text{Radiation}^b \cdot [SO_2]^c \cdot (CS \cdot RH)^f$	$a = 8.21 \times 10^{-3}$, $b = 1$, $c = 0.62$, $f = -0.13$	Mikkonen et al. (2011)
$\text{Proxy}_{\text{Lu et al.}}$	$k_0 \cdot UVB^a \cdot [SO_2]^b \cdot CS^c \cdot \left(O_3{}^d + NO_x^f\right)$	$k_0 = 0.0013$, $a = 0.13$, $b = 0.40$, $c = -0.17$, $d = 0.44$, $f = 0.41$	Lu et al. (2019)
$\text{Proxy}_{\text{Lubna et al.}}$	$\frac{CS}{2k_3} + \sqrt{\left(\frac{CS}{2k_3}\right)^2 + \frac{[SO_2]}{k_3} k_1 Glob}$	$k_1 = 1.0 \times 10^{-6}$, $k_3 = 1.6 \times 10^{-7}$	Dada et al. (2020)

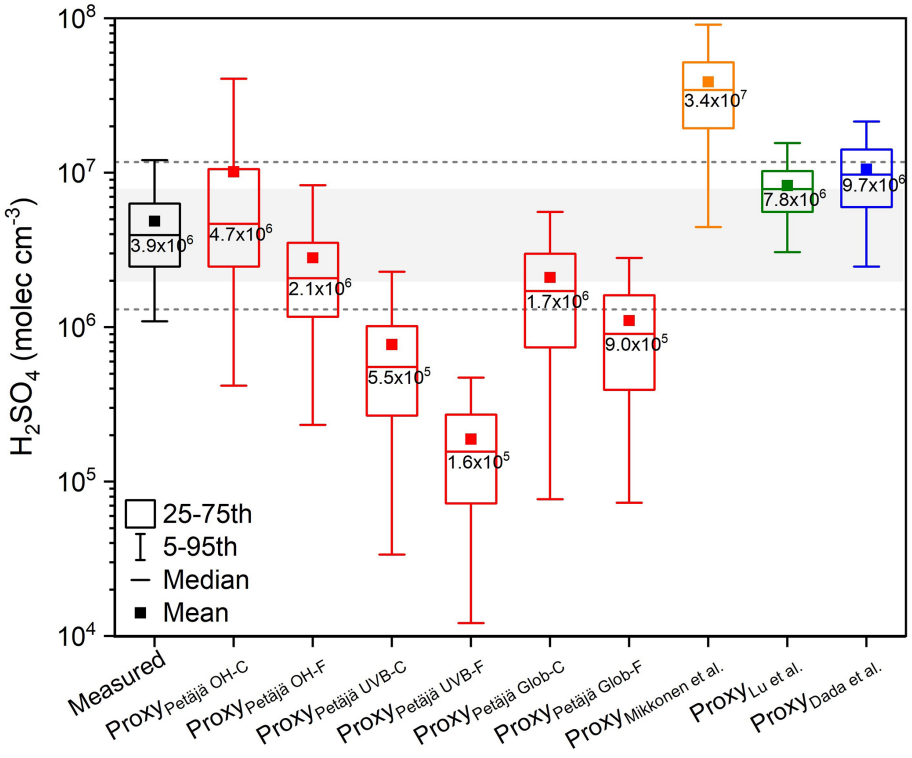

Figure 3. Sulfuric acid concentrations from measurement and estimated by proxies from literatures during the time window of 10:00–14:00 LT in 2019 (1 January to 31 December). Black value inside each box is the median concentration. "$Proxy_{Petäjä\ OH–C}$" "$Proxy_{Petäjä\ OH–F}$" "$Proxy_{Petäjä\ UVB–C}$" "$Proxy_{Petäjä\ UVB–F}$" "$Proxy_{Petäjä\ Glob–C}$" and "$Proxy_{Petäjä\ Glob–F}$" represent sulfuric acid proxies from the work of Petäjä et al. (2009), with P_1 proxy using OH radical with constant pre-factor k_1, P_1 proxy using OH radical with fitted pre-factor k_1, P_2 proxy using UVB with constant pre-factor k_2, P_2 proxy using UVB with fitted pre-factor k_2, P_3 proxy using global radiation with constant pre-factor k_3, and P_3 proxy using global radiation with fitted pre-factor k_3, respectively. "$Proxy_{Mikkonen\ etāl.}$" "$Proxy_{Lu\ et\ al.}$" and "$Proxy_{Dada\ et\ al.}$" are sulfuric acid proxies from the work of Mikkonen et al. (2011), Lu et al. (2019) and Dada et al. (2020), respectively. Gray area covers 50 % to 200 % of median concentration of measured sulfuric acid, and two gray lines cover 33.3 % to 300 % of median concentration of measured sulfuric acid.

Table 4. The correlation coefficients (R), power exponents (Exponent) and slopes (Linear Slope) of the linear fittings between measured sulfuric acid concentration and the estimated ones using proxies from literatures, the relative errors (RE) of the estimated sulfuric acid concentrations to the measured one, as well as the ratios of proxy concentrations to measured concentration using mean ($[Proxy/Measured]_{mean}$) and median ($[Proxy/Measured]_{median}$) values. All parameters are fitted with Bisquare fitting. Bold values denote that, for corresponding parameters, the sulfuric acid proxies perform well.

Proxy	R	Exponent	Linear slope	RE (%)	$[Proxy/Measured]_{mean}$	$[Proxy/Measured]_{median}$	References
$Proxy_{Petäjä\ OH–C}$	**0.97**	**1.17**	**0.85**	74 %	**2.09**	**1.18**	Petäjä et al. (2009)
$Proxy_{Petäjä\ OH–F}$	**0.78**	**0.80**	0.30	**35 %**	**0.58**	**0.53**	
$Proxy_{Petäjä\ UVB–C}$	**0.84**	**1.08**	0.09	57 %	0.16	0.14	
$Proxy_{Petäjä\ UVB–F}$	0.52	0.63	0.01	64 %	0.04	0.04	
$Proxy_{Petäjä\ Glob–C}$	0.59	**0.86**	0.16	**40 %**	**0.43**	**0.43**	
$Proxy_{Petäjä\ Glob–F}$	0.44	0.57	0.05	50 %	0.23	0.23	
$Proxy_{Mikkonen\ etāl.}$	0.46	0.49	2.40	565 %	7.98	8.70	Mikkonen et al. (2011)
$Proxy_{Lu\ et\ al.}$	0.38	0.30	0.42	91 %	**1.70**	**1.99**	Lu et al. (2019)
$Proxy_{Dada\ et\ al.}$	0.18	0.30	0.45	133 %	2.17	2.46	Dada et al. (2020)

As shown in Fig. 3 and Table 4, estimated sulfuric acid concentrations from $\text{Proxy}_{\text{Petäjä OH–C}}$, $\text{Proxy}_{\text{Petäjä OH–F}}$ and $\text{Proxy}_{\text{Lu et al.}}$ are closest to the measured one, with median deviations within twofold. This suggests that these three proxies provide the best estimates of sulfuric acid concentration. Estimated sulfuric acid concentrations from $\text{Proxy}_{\text{Petäjä Glob–C}}$ and $\text{Proxy}_{\text{Dada et al.}}$ are not too far away from the measured one, with median deviations within threefold. While estimated concentrations from other proxies differ substantially from the measured one, especially $\text{Proxy}_{\text{Petäjä UVB–F}}$, which underestimates sulfuric acid concentration markedly. The linear correlation coefficients of $\text{Proxy}_{\text{Petäjä OH–C}}$, $\text{Proxy}_{\text{Petäjä OH–F}}$ and $\text{Proxy}_{\text{Petäjä UVB–C}}$ proxies are closet to 1.0. Similarly, the power exponents of $\text{Proxy}_{\text{Petäjä OH–C}}$, $\text{Proxy}_{\text{Petäjä OH–F}}$, $\text{Proxy}_{\text{Petäjä UVB–C}}$ and $\text{Proxy}_{\text{Petäjä Glob–C}}$ are closet to 1.0. This indicates that the estimated sulfuric acid from former three proxies have the best linear correlation with the measurement. Only the slope of $\text{Proxy}_{\text{Petäjä OH–C}}$ (0.85) is close to 1.0, suggesting that it performs the best in linear relationship. For $\text{Proxy}_{\text{Petäjä UVB–F}}$, $\text{Proxy}_{\text{Petäjä Glob–F}}$, $\text{Proxy}_{\text{Mikkonen et al.}}$, $\text{Proxy}_{\text{Lu et al.}}$ and $\text{Proxy}_{\text{Dada et al.}}$, none of the linear correlation coefficients, power exponents or the slopes perform well, indicating that they fail to reproduce the linearity with measured sulfuric acid. The relative errors are within 50 % for $\text{Proxy}_{\text{Petäjä OH–F}}$, $\text{Proxy}_{\text{Petäjä Glob–C}}$ and $\text{Proxy}_{\text{Petäjä Glob–F}}$, and those for $\text{Proxy}_{\text{Petäjä OH–C}}$, $\text{Proxy}_{\text{Petäjä UVB–C}}$, $\text{Proxy}_{\text{Petäjä UVB–F}}$ and $\text{Proxy}_{\text{Lu etāl.}}$ range from 57 % to 91 %.

Considering both linear correlation and concentration estimation accuracy, $\text{Proxy}_{\text{Petäjä OH–C}}$ and $\text{Proxy}_{\text{Petäjä OH–F}}$ are the two most suitable proxies for reproducing sulfuric acid concentration. Other four proxies from Petäjä et al. (2009) without the OH radical term underestimate the concentration of sulfuric acid. The reason might be that the scaling factors k_2 and k_3 were obtained by fitting measured sulfuric acid and other parameters rather than deriving from the direct relationships between UVB/global radiation and OH radical. Under this circumstance, scaling factors k_2 and k_3 are influenced by measured sulfuric acid, UVB and global radiation as well as calculated CS, which may introduce substantial uncertainties. Moreover, for both concentration estimation and linearity (R, exponent and linear slope), proxies with fitted scaling factors performed worse that those with constant scaling factors. This may be due to the absence of linear relationships between proxies and photochemical terms (OH radical, UVB, or global radiation), since the fitted scaling factors k_1, k_2 and k_3 all include the photochemical term (Table 3).

Note that the scaling factor k_1 of the OH-based proxy was obtained by replacing the left hand side of the equation with measured sulfuric acid concentration (Petäjä et al., 2009). Thus, k_1 was not derived from the chemical production pathways of sulfuric acid, and the best-fit value of k_1 may vary from site to site. This limitation restricts its applicability across a broader range of sites. Therefore, in this study, we aim to derive a proxy based entirely on the formation and loss pathways of sulfuric acid, where the parameters, related pre-factors and exponents all have chemical and physical meanings. Proxies of this kind should be applicable across different sites, since no site-dependent scaling factors or exponents are used.

3.3 Derivation of sulfuric acid proxies from its budget analysis

During daytime, the main formation pathway of sulfuric acid is the SO_2 oxidation by OH radical, followed by O_2 and H_2O addition (Reactions R1–R3) (Finlayson-Pitts and Pitts, 2000):

$$SO_2 + OH \xrightarrow{k_1} HSO_3 \quad \text{(R1)}$$

$$HSO_3 + O_2 \xrightarrow{k_2} SO_3 + HO_2 \quad \text{(R2)}$$

$$SO_3 + 2H_2O \xrightarrow{k_3} H_2SO_4 + H_2O. \quad \text{(R3)}$$

As OH radical oxidation is the rate-limiting step, the production rate of sulfuric acid is nearly equivalent to that of HSO_3 and can be calculated as follows:

$$P_{[H_2SO_4]} = P_{[HSO_3]} = k_1 \cdot [SO_2] \cdot [OH]. \quad (10)$$

Regarding sulfuric acid losses, the main loss pathway is its condensation sink onto particle surfaces (Dada et al., 2020; Guo et al., 2021; Yang et al., 2021a), which can be written as:

$$L_{[H_2SO_4]} = [H_2SO_4] \cdot CS. \quad (11)$$

The production and loss rates of sulfuric acid are much faster than its net concentration change (Guo et al., 2021), so a pseudo-steady-state assumption can be applied:

$$k_1 \cdot [SO_2] \cdot [OH] \approx [H_2SO_4] \cdot CS. \quad (12)$$

Then, the steady-state concentration of sulfuric acid can be estimated, which can be called as the OH–CS based proxy:

$$\text{Proxy}_{\text{OH,CS}} = [H_2SO_4] = \frac{k_{SO_2\text{–OH}} \cdot [SO_2] \cdot [OH]}{CS}. \quad (13)$$

Here, $k_{SO_2\text{–OH}}$ is the rate constant of SO_2 oxidation by OH adical. It is taken as $1.3 \times 10^{-12}(T/300)^{-0.7}$ cm^3 s^{-1}, where T is the temperature in Kelvin (Wine et al., 1984; Atkinson et al., 2004), $[SO_2]$ and [OH] are concentrations of SO_2 and OH radical in molec. cm^{-3}, and CS is condensation sink of sulfuric acid in s^{-1}. Compared with the proxy proposed by Petäjä et al. (2009), the pre-factor $k_{SO_2\text{–OH}}$ is not obtained by parameter fitting but is a verified reaction coefficient derived from experiments. Therefore, this proxy is chemically meaningful and has the potential to be used at various sites.

It is widely acknowledged that the OH radical is difficult to measure. Therefore, for most sites lacking OH radical measurements, the OH–CS based proxy cannot be applied. A major production pathway for OH radical is the photolysis of NO_2 and O_3, along with radical recycling (Lu et al., 2012; Ma et al., 2022), all driven by solar radiation (Rohrer and Berresheim, 2006). Thus, UVB, a readily available parameter, can replace [OH] in Eq. (13) to derive the second proxy as follows:

$$\mathrm{Proxy}_{\mathrm{UVB,CS}} = \frac{k_{\mathrm{UVB-CS}} \cdot [\mathrm{SO_2}] \cdot \mathrm{UVB}}{\mathrm{CS}} \quad (14)$$

where $k_{\mathrm{UVB-CS}}$ is the pre-factor, and $[SO_2]$, UVB, and CS are in the units of molec. cm^{-3}, W m^{-2} and s^{-1}, respectively. As shown in Fig. S7a, OH radical and UVB has a linear correlation with R value of 0.86. The ratio of OH radical to UVB is 6.14×10^6 molec. cm^{-3} W^{-1} m^2. Accounting for this ratio yields $k_{\mathrm{UVB-CS}}$ of $7.98 \times 10^{-6}(T/300)^{-0.7}$ W^{-1} m^2 s^{-1}. Replacing the left hand side of Eq. (14) with measured sulfuric acid concentration yields $k_{\mathrm{UVB-CS}}$ of $7.5 \times 10^{-6}(T/300)^{-0.7}$ W^{-1} m^2 s^{-1}, which is close to the value derived from the OH–UVB relationship. This $k_{\mathrm{UVB-CS}}$ is finally used as it brings less deviation between measured and estimated sulfuric acid concentrations.

Furthermore, calculating CS requires particle size distribution data, which is not always available. In this case, a surrogate parameter for CS is needed. The condensation sink of gaseous species onto particles is mainly determined by the aerosol surface area. $PM_{2.5}$ measures the masses of particles. In principle, CS and $PM_{2.5}$ should follow a power-law relationship with an exponent of 2/3. As expected, $PM_{2.5}^{2/3}$ and CS are well linearly correlated (Fig. S7b, $R = 0.92$). Thus, replacing CS in Eq. (14) with $PM_{2.5}^{2/3}$ yields the third proxy as follows:

$$\mathrm{Proxy}_{\mathrm{UVB,PM_{2.5}}} = \frac{k_{\mathrm{UVB}text--\mathrm{PM_{2.5}}} \cdot [\mathrm{SO_2}] \cdot \mathrm{UVB}}{\mathrm{PM}_{2.5}^{2/3}} \quad (15)$$

where $k_{\mathrm{UVB-PM_{2.5}}}$ is the pre-factor, and $[SO_2]$, UVB, and $PM_{2.5}$ are in the units of molec. cm^{-3}, W m^{-2} and $\mu g\, m^{-3}$, respectively. The slope of CS to $PM_{2.5}^{2/3}$ is 2.67×10^{-3} s^{-1} $\mu g^{-2/3}$ m^2. Then, substituting [OH] with UVB and CS with $PM_{2.5}^{2/3}$ yields $k_{\mathrm{UVB-PM_{2.5}}}$ of 2.99×10^{-3} $\mu g^{2/3}$ W^{-1}. Replacing the left hand side of Eq. (15) with measured sulfuric acid concentration yields $k_{\mathrm{UVB-PM_{2.5}}}$ of 2.8×10^{-3} $\mu g^{2/3}$ W^{-1}, which is close to the value derived from the OH–UVB and CS–$PM_{2.5}$ relationships and is finally used.

We summarize the three proxies incorporating the corresponding parameters as follows:

$$\mathrm{Proxy}_{\mathrm{OH,CS}} = \left(1.3 \times 10^{-12}\right) \times \left(\frac{T}{300}\right)^{-0.7} \times [\mathrm{SO_2}] \times [\mathrm{OH}] \div \mathrm{CS} \quad (16)$$

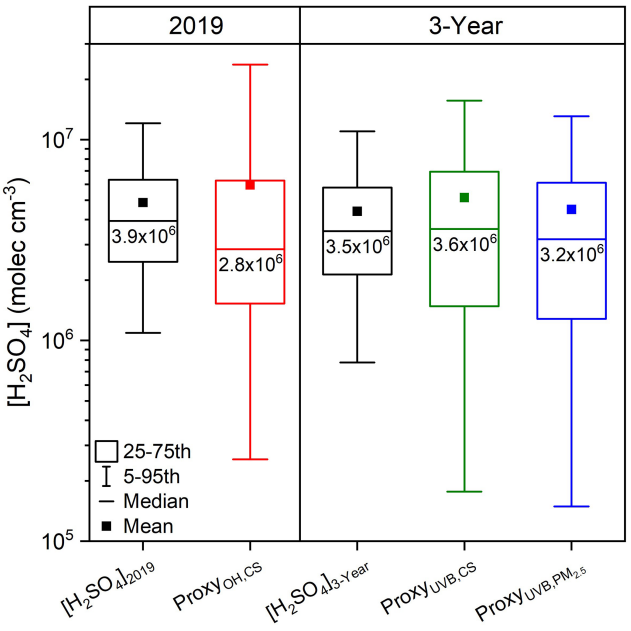

Figure 4. Sulfuric acid concentrations from measurement and estimated by proxies in this study during daytime (10:00–14:00 LT).

$$\mathrm{Proxy}_{\mathrm{UVB,CS}} = \left(7.5 \times 10^{-6}\right) \times \left(\frac{T}{300}\right)^{-0.7} \times [\mathrm{SO_2}] \times \mathrm{UVB} \div \mathrm{CS} \quad (17)$$

$$\mathrm{Proxy}_{\mathrm{UVB,PM_{2.5}}} = \left(2.8 \times 10^{-3}\right) \times [\mathrm{SO_2}] \times \mathrm{UVB} \div \mathrm{PM}_{2.5}^{2/3}. \quad (18)$$

The uncertainties of the OH–CS, UVB–CS, and UVB–$PM_{2.5}$ based proxies, based on Eqs. (16)–(18), are estimated to be 41.7 %, 96.1 %, and 100.4 %, respectively. Details are provided in Sect. S3.

3.4 Evaluation of different sulfuric acid proxies in this study

3.4.1 Performance of sulfuric acid proxies at Beijing Site

Figure 4 shows the overall concentrations of measured and estimated sulfuric acid from proxies. The estimated sulfuric acid concentrations from three proxies are generally in good agreement with the measured one, although the OH–CS-based proxy yields slightly lower concentration than measurement. Additionally, the concentration ranges estimated by proxies are broader than the measured one. Detailed sulfuric acid concentrations, including mean, standard deviation, median, lower quartile and upper quartile values are summarized in Table S4.

The scatter plots of three proxies vs. measured sulfuric acid are shown in Fig. 5. For all three proxies, the estimated sulfuric acid concentrations are well correlated with

Table 5. The correlation coefficients (R) and power exponents (Exponent) of the linear fittings between measured sulfuric acid concentration and the estimated ones using proxies in this study, the relative errors (RE) of the estimated sulfuric acid concentrations to the measured one, as well as the ratios of proxy concentrations to measured concentration using mean ([Proxy/Measured]$_{mean}$) and median ([Proxy/Measured]$_{median}$) values.

Year	Parameters	R	Exponent	RE (%)	[Proxy/Measured]$_{mean}$	[Proxy/Measured]$_{median}$
2019	$Proxy_{OH,CS}$	0.96	1.14	46 %	1.22	0.72
3-Year	$Proxy_{UVB,CS}$	0.83	1.02	32%	1.17	1.03
	$Proxy_{UVB,PM_{2.5}}$	0.79	1.02	40 %	1.02	0.91

the measured one, with most data points falling on or near the 1 : 1 line. This suggests that the three steady-state based proxies generally perform well in estimating daytime sulfuric acid concentration. However, slight deviations between the least-square-fit lines and the 1 : 1 lines can be observed. To better understand these deviations, we summarize the correlation coefficients and power exponents of the fits between measured and estimated sulfuric acid concentrations, as well as the relative errors of the estimated concentrations (Table 5). The OH–CS-based proxy shows the best correlation ($R = 0.96$). The R values for the UVB–CS based proxy (0.83) and the UVB–$PM_{2.5}$ based proxy (0.79) are also close to unity. The OH–CS based proxy has an exponent of 1.14, indicating that the relationship between proxy and measured sulfuric acid is not strictly linear, which could, to some extent, arise from the uncertainty in OH radical modelling. The exponents of UVB–CS based proxy (1.02) and UVB–$PM_{2.5}$ based proxy (1.02) are very close to 1.0, suggesting excellent good linear relationships between proxies measured sulfuric acid. The relative errors of three proxies are all within 50 %, which performs better than most proxies from previous studies (Table 4). Moreover, the ratios of proxy to measured concentrations give the same result that they are in the range of 0.72–1.22, much closer to 1.0 than most proxies from previous studies (Table 4). It should be pointed out that, as the time window moves further from noon, the OH–CS based proxy increasingly underestimates the sulfuric acid concentration. And as the time window shifts away from noon, the relationship between proxy and measured sulfuric acid becomes increasingly nonlinear. This implies that in the early morning or at nightfall, sulfuric acid sources other than OH + SO_2 pathway cannot be neglected (Fig. S15).

To have better understanding on the performance of sulfuric acid proxies at any given moment, the time variations of sulfuric acid concentrations from three proxies and measurement are shown in Figs. S8 and S9. Generally, the OH–CS based proxy provides a good estimation on daytime sulfuric acid concentration (Fig. S8). Specifically, in 2019, the concentration estimated by this proxy matches well with the measured one in January, February, March, April, August, and September. In other months of 2019, it underestimates or overestimates sulfuric acid concentration. This shows that although the OH–CS-based proxy generally performs well, sulfuric acid concentration at a given moment may deviate. Similarly, sulfuric acid concentrations estimated by UVB–CS based and UVB–$PM_{2.5}$ based proxies generally match well with the measured one at most of the daytime, with deviations noticeable in several months over 3 years (Figs. S8 and S9). These time variations are consistent with the findings in Sect. 3.1.2: the daily peak width of OH–CS based proxy is narrower than that of measured sulfuric acid, and the daily peak widths of UVB–CS based and UVB–$PM_{2.5}$ based proxies are narrower than that of OH–CS based proxy. Furthermore, the OH–CS based proxy partially reproduces the formation of sulfuric acid at night and early morning, with evidence on most days of January 2019 and some days of February 2019. Although UVB–CS based and UVB–$PM_{2.5}$ based proxies cannot estimate nighttime sulfuric acid, they provide a convenient, reliable and, more importantly, feasible way to trace the long-term daytime sulfuric acid concentration for sites without OH radicals.

Sulfuric acid concentration is estimated using OH radical, UVB, SO_2, CS and $PM_{2.5}$. We then use these parameters to assess how well the proxy-estimated concentrations match the measured values, and to determine the applicable parameter ranges of the proxies. Figure 6 shows that when [OH] is lower than 4×10^5 molec. cm^{-3}, UVB is lower than 0.10 W m^{-2} or SO_2 is lower than 0.5 ppb, all three steady-state based proxies underestimate sulfuric acid concentration. This suggests that when the OH radical, UVB, or SO_2 is low, other SO_2 oxidation pathways or additional sulfuric acid sources contribute more to sulfuric acid formation. As [OH] increases, the ratio of proxy to measured sulfuric acid gradually rises above 1.0. These deviations of OH–CS based proxy may arise from uncertainties in OH radical modelling. As UVB and SO_2 increase, the ratios of proxies to measured sulfuric acid stabilize around 1.0. This suggests that although the OH–CS based proxy is derived entirely from sulfuric acid budget analysis, its long-term stability may not be as good as that of UVB–CS based or UVB–$PM_{2.5}$ based proxies, given the intrinsic uncertainty in OH modeling. The ratio of UVB–CS based proxy stays around 1.0 when CS is lower than 0.07 s^{-1}, accounting for ∼ 96.3 % of total data. Similarly, the

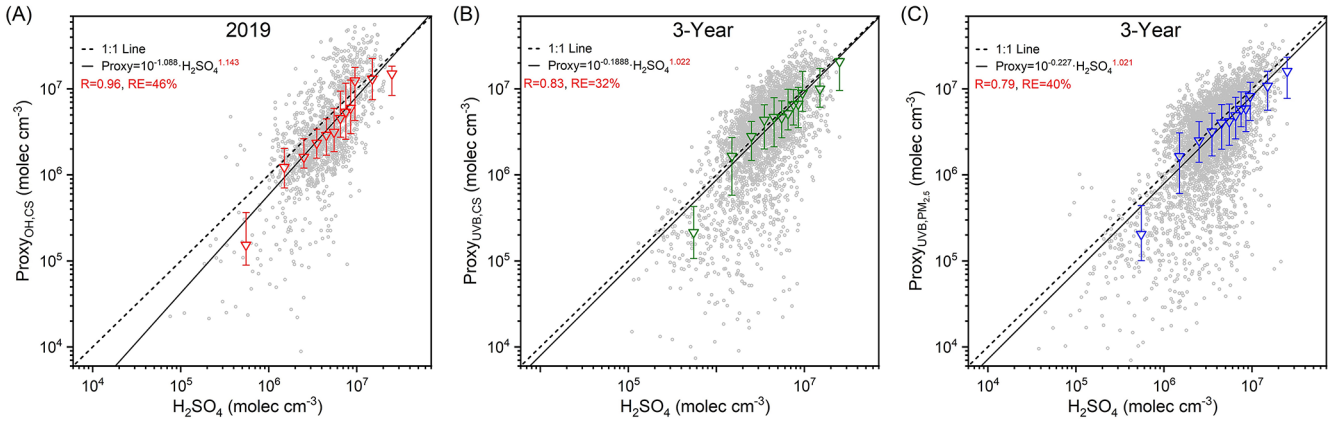

Figure 5. Sulfuric acid concentrations estimated by proxies in this study vs. the measured concentration during daytime (10:00–14:00 LT) for **(a)** OH–CS based proxy in 2019, **(b)** UVB–CS based proxy in 3 years, and **(c)** UVB–$PM_{2.5}$ based proxy in 3 years. The black dashed lines are 1 : 1 lines, and the black lines are the distance weighted least square fits between proxy and measured sulfuric acid. Corresponding functions of the fits, correlation coefficients (R) and relative errors (RE) are shown in the legend. The triangle marker represents the binned data, where the up line, middle marker and bottom lines stand for upper quartile, median and lower quartile, respectively.

ratio of UVB–$PM_{2.5}$ based proxy shows no clear dependence on $PM_{2.5}$ when it is lower than 200 $\mu g\,m^{-3}$, accounting for $\sim$ 99.6 % of all datasets. This indicates that these two proxies can be applied across almost all CS and $PM_{2.5}$ ranges. For OH–CS based proxy, sulfuric acid concentration is underestimated when CS is lower than 0.015 s^{-1} ($\sim$ 32.2 %) or higher than 0.07 s^{-1} ($\sim$ 3.6 %). Higher CS is also associated with more polluted conditions when other sulfuric acid sources such as primary emissions may exist (Yang et al., 2021a). At lower CS, UVB–CS based proxy performs well, while OH–CS based proxy does not, suggesting that slightly poor performance of OH–CS based proxy may arise from OH radical modelling. Meanwhile, the performances of three steady-state based proxies show a clear dependence on RH. When RH is lower than 60 %, the ratios of proxies to measured sulfuric acid stabilize around 1.0. When RH exceeds 60 % ($\sim$ 13.6 % of total data), these ratios increase with RH. Higher RH correlates with precipitation events with lower UVB and lower SO_2, increasing the contribution of additional sulfuric acid sources. This may partly explain the underestimation of proxies at higher RH.

Sulfuric acid is a key precursor in NPF processes. Therefore, it is necessary to assess how well these proxies perform during NPF periods. As shown in Figs. 6 and S10, about 30 % of NPF cases fall outside the optimal range of SO_2, while most NPF cases fall within the optimal ranges of OH radical, UVB, CS, $PM_{2.5}$, and RH. Consequently, during NPF periods, the performance of three proxies mainly depends on the SO_2 concentration at that time. As shown in Fig. S11, restricting the analysis to data within the optimal parameter ranges reduces the number of data points that deviate from the 1 : 1 line and have extremely low estimated sulfuric acid concentrations. Meanwhile, the correlation coefficients between the estimated and measured sulfuric acid concentrations generally improved, while the relative errors increased, and the improvement in the slopes of linear fits was not significant. This suggests that data outside the optimal parameter ranges generally have little impact on the fitting results.

3.4.2 Performance of sulfuric acid proxies at Hyytiälä, Finland

Because the three proxies above are derived from the budget analysis of sulfuric acid, Eqs. (16)–(18) and their pre-factors should be applicable to other sites. To demonstrate this, we use datasets from a boreal forest site in Hyytiälä, Finland as test data. Figure 7 shows the scatter plots of UVB–CS based and UVB–$PM_{2.5}$ based proxies vs. measured sulfuric acid. For both proxies, most data points lie on or are near the 1 : 1 line, with R values close to 1.0, indicating good linear correlations between the estimated and measured sulfuric acid concentrations. The relative errors for UVB–CS based and UVB–$PM_{2.5}$ based proxies of Hyytiälä site are 97 % and 80 %, respectively, which are only slightly larger than those of the Beijing site (Table 5) but still within an acceptable range. The above results suggest that both proxies perform well in estimating daytime sulfuric acid concentration at Hyytiälä.

For the UVB–CS based proxy, the pre-factor $k_{\mathrm{UVB–CS}}$ in Eq. (17) was chosen the same as Beijing. This proxy estimates sulfuric acid concentrations well at both Beijing and Hyytiälä sites using the same $k_{\mathrm{UVB–CS}}$ value, indicating that the OH–UVB relationships, or the k' values in $[\mathrm{OH}] = k' \cdot \mathrm{UVB}$, do not differ significantly between these two sites. This further suggests that k' values at other sites should not differ significantly, and that $k_{\mathrm{UVB–CS}}$ values should be similar across sites.

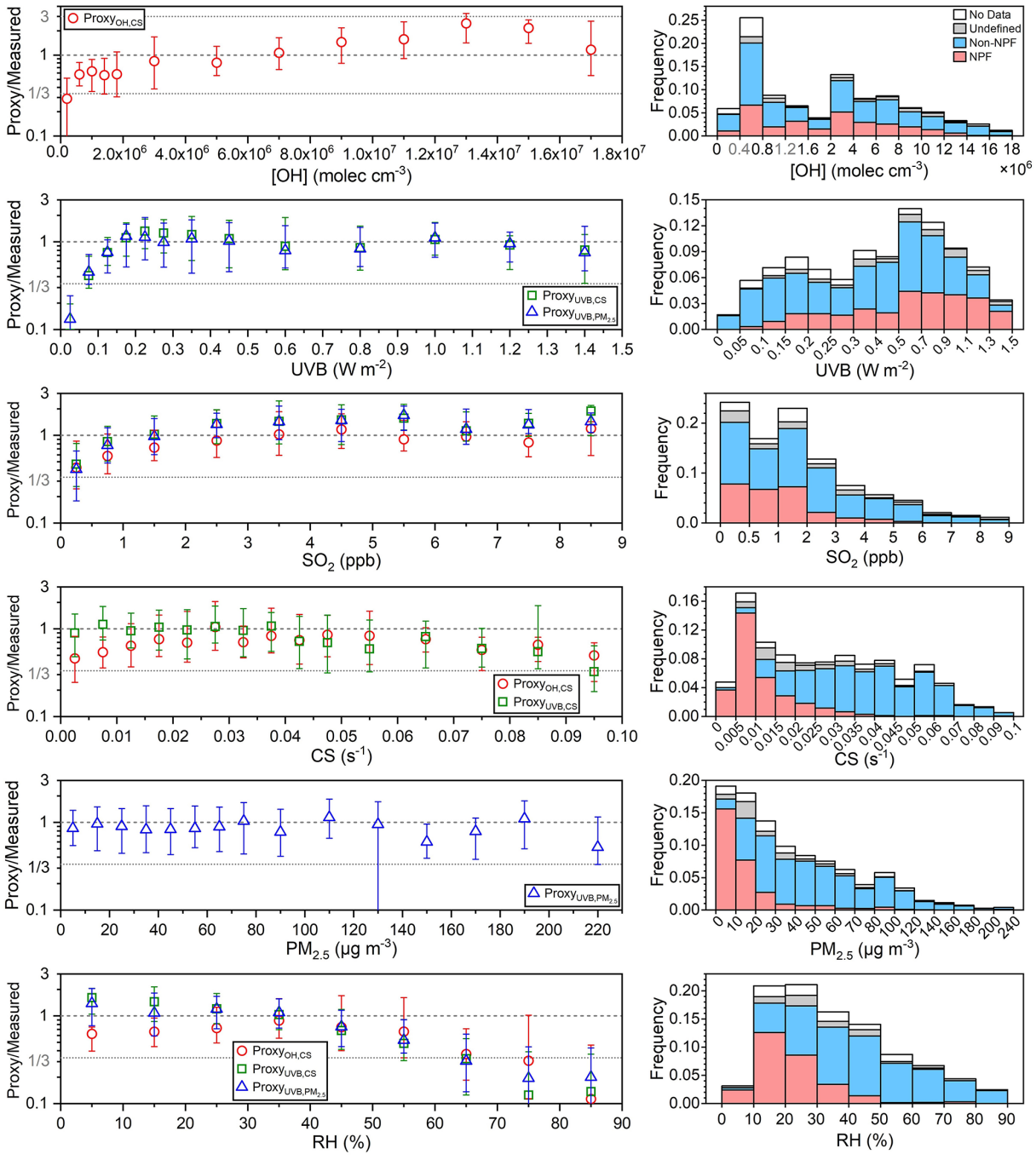

Figure 6. Left panels: the ratios of sulfuric acid concentrations estimated by proxies in this study to the measured one (Proxy/Measured) vs. concentration of OH radical ([OH]), UVB, SO_2, CS, $PM_{2.5}$ and RH during daytime (10:00–14:00 LT) of 2019. Different colored markers represent different proxies. The up line, middle marker and bottom line stand for upper quartile, median and lower quartile values respectively. Right panels: frequency distributions of corresponding parameters classified by "NPF", "Non-NPF", "Undefined", and "No Data" periods.

For the UVB–$PM_{2.5}$ based proxy, the pre-factors $k_{\mathrm{UVB–PM_{2.5}}}$ in Eq. (18) are 2.8×10^{-3} $\mu g^{2/3}$ W^{-1} and 4.7×10^{-3} $\mu g^{2/3}$ W^{-1} for Beijing and Hyytiälä, respectively. This difference in $k_{\mathrm{UVB\text{-}PM_{2.5}}}$ arises from the disparity of pre-factor in $\mathrm{CS} = k \cdot \mathrm{PM}_{2.5}^{2/3}$, where the values of k are 2.67×10^{-3} s^{-1} $\mu g^{-2/3}$ m^2 and 1.59×10^{-3} s^{-1} $\mu g^{-2/3}$ m^2 for Beijing (Fig. S7b) and Hyytiälä (Fig. S12a), respectively. Specifically, the ratios of 4.7×10^{-3} to 2.8×10^{-3} and of 2.67×10^{-3} to 1.59×10^{-3} are both 1.68. Therefore, considering the CS–$PM_{2.5}$ relationships, Eq. (18) is also applicable to Hyytiälä. This tells us that when using the UVB–

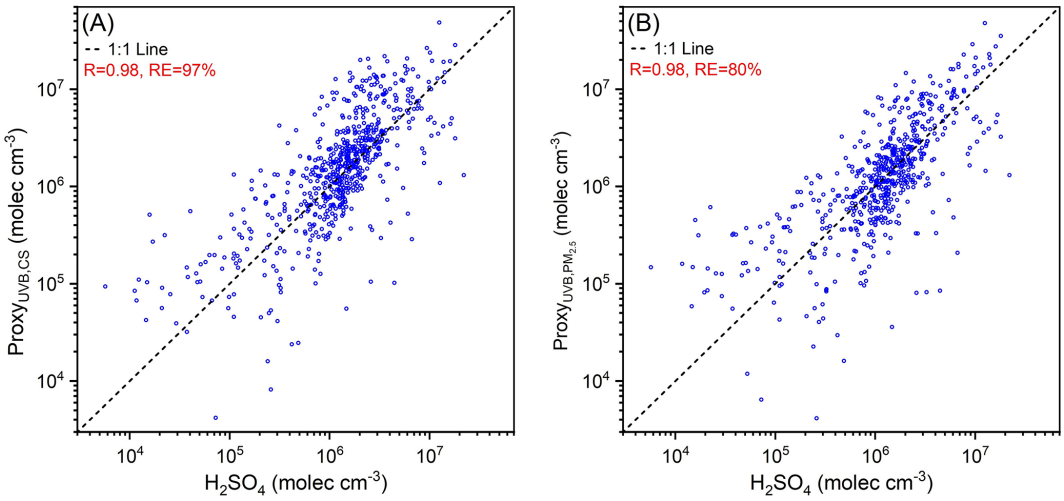

Figure 7. **(a)** UVB–CS based proxy ($Proxy_{UVB,CS}$) and **(b)** UVB–$PM_{2.5}$ based proxy ($Proxy_{UVB,PM_{2.5}}$) vs. measured sulfuric acid of Hyytiälä, Finland during daytime (10:00–14:00 LT) from 8 March to 13 August 2018. The pre-factor of $Proxy_{UVB,CS}$ ($k_{UVB,CS}$) is $7.5 \times 10^{-6}(T/300)^{-0.7}$ W^{-1} m^2 s^{-1}, which is the same as Beijing. The pre-factor of $Proxy_{UVB,PM_{2.5}}$ ($k_{UVB,PM_{2.5}}$) is 4.7×10^{-3} μg$^{2/3}$ W^{-1}. In both two plots, the black dashed lines are 1 : 1 lines. Correlation coefficients (R) and the relative errors (RE) are shown in the legend.

$PM_{2.5}$ based proxy to estimate sulfuric acid concentration, the k value should be determined first to correct $k_{UVB-PM_{2.5}}$. Moreover, this coefficient k for one Nanjing site is 1.62×10^{-3} s^{-1} μg$^{-2/3}$ m^2 (Fig. S16), which falls between those of Beijing and Hyytiälä. This implies that although the values of k vary among sites, this difference remains modest. Figure S8b and c shows that the slope of CS to $PM_{2.5}^{2/3}$ is stable across years and seasons at a given site. Therefore, by conducting short-term synchronous measurement of $PM_{2.5}$ and particle size distribution, a reliable k can be obtained. In summary, these steady-state based proxies are transferable proxies that can be widely used to estimate daytime sulfuric acid concentration at other atmospheric sites.

4 Summary and conclusions

In this study, long-term measurement of sulfuric acid from 2019 to 2021 was conducted in urban Beijing. Daytime sulfuric acid concentration ranges from 2.0×10^6 to 7.4×10^6 molec. cm^{-3} and shows a general declining trend, with an average annual decrease of 14 %, which is mainly due to SO_2 reduction. In addition, sulfuric acid concentration shows a clear seasonal variation that tracks UVB, reaching the highest in May and September and decreasing to the lowest from November to February of next year. In July and August, frequent precipitation lowers UVB and SO_2, resulting in lower sulfuric acid. Nighttime sulfuric acid concentration ranges from 1.6×10^5 to 6.3×10^5 molec. cm^{-3}, about one order of magnitude lower than daytime. In warmer seasons, the sources of nighttime sulfuric acid, such as benzene-related emissions and alkene ozonolysis, are stronger, and the losses are weaker, leading to higher sulfuric acid level. The diurnal variations of photo-oxidation related parameters deviate slightly from sulfuric acid. Sulfuric acid peaks earliest, followed by $J(NO_2)$, $J(O^1D)$, UVB, global radiation, and OH radical. Meanwhile, the peak width of sulfuric acid is the widest, followed by $J(NO_2)$, global radiation, OH radical, $J(O^1D)$, and UVB.

The challenges in sulfuric acid measurement hinder its widespread observation. To obtain sulfuric acid proxies applicable to most sites, we derive three sulfuric acid proxies directly from its steady-state budget analysis, named as OH–CS based, UVB–CS based, and UVB–$PM_{2.5}$ based proxies. All three proxies perform well in estimating sulfuric acid concentration during 10:00–14:00 LT. We also evaluate the performance of nine sulfuric acid proxies proposed in previous studies: seven based on formation and loss pathways (Petäjä et al., 2009; Dada et al., 2020) and two derived from numerical regression (Mikkonen et al., 2011; Lu et al., 2019). Results show that $Proxy_{Petäjä\ OH–C}$ and $Proxy_{Petäjä\ OH–F}$ generally reproduce daytime sulfuric acid concentrations well, with estimated concentrations closet to the measured one, correlation coefficients being 0.97 and 0.78, respectively, and relative errors being 74 % and 35 %, respectively. However, the scaling factors therein are obtained by fitting the proxy equations. Thus, these scaling factors are influenced by measurement reliability and have limited applicability at other sites. By contrast, our proxies are derived directly from sulfuric acid budget analysis, and the parameters in the proxy equations are transferable that can be used at a boreal forest site in Hyytiälä, Finland. Therefore, the three proxies developed in this study have high potential for estimating daytime sulfuric acid concentrations at various sites.

It should be noted that the OH radical used in this study is not measured, but derived from a model simulation. Under this circumstance, the OH–CS based proxy generally performs well, but has some deviations when OH radical is in the range of $1.2–1.6 \times 10^7$ molec. cm^{-3} and CS is lower than $0.015\ s^{-1}$. Although three steady-state-based proxies generally perform well, they are not suitable under certain conditions. When OH radical, UVB and SO_2 are too low, when CS and $PM_{2.5}$ are too high, or when RH exceeds 60 %, estimated sulfuric acid concentration may deviate from the actual concentration to a larger extent. Moreover, three proxies cannot fully reproduce sulfuric acid concentration in early morning and at nightfall. This indicates that during these two periods, other sulfuric acid sources, such as direct emission, alkenes ozonolysis and other formation pathways, are also important.

Here are some suggestions for the selection of three proxies. If one site has comprehensive measurement of OH radical, particle size distribution and SO_2, the OH–CS based proxy illustrated by Eq. (16) is preferred, since it estimates daytime concentration well and partly captures diurnal variation and nighttime sulfuric acid. Moreover, the pre-factor in Eq. (16) is the actual $OH + SO_2$ reaction rate, making it suitable to all atmospheric sites. Then, if OH radical is not directly measured, but UVB, SO_2, and particle size distribution are available, the UVB–CS based proxy illustrated by Eq. (17) is preferred. Although it cannot perfectly trace the diurnal variation of sulfuric acid, it estimates daytime concentration well. Moreover, because its pre-factor is transferable, it is convenient and straightforward to use. Finally, if neither OH radical nor particle size distribution is measured, but UVB, SO_2, and $PM_{2.5}$ are available, the UVB–$PM_{2.5}$ based proxy should be the right choice. These three parameters used are commonly measured, giving this proxy broad applicability. Noted that $k_{\mathrm{UVB–PM_{2.5}}}$ in Eq. (18) various across sites. For better accuracy, short-term synchronous measurement of particle size distribution and $PM_{2.5}$ is suggested for obtaining the pre-factor (k) in $CS = k \cdot PM_{2.5}^{2/3}$ and then correcting $k_{\mathrm{UVB–PM_{2.5}}}$.

The acquisition of fundamental sulfuric acid concentration datasets is of great significance for elucidating the global spatial distribution and long-term temporal trends of sulfuric acid. This may further promote researches on the mechanisms of atmospheric nucleation, cluster growth, secondary aerosol formation, and pollution event evolution at corresponding regions.

Data availability. Datasets for this paper can be accessed at https://doi.org/10.5281/zenodo.17216660 (Guo et al., 2025).

Supplement. The supplement related to this article is available online at https://doi.org/10.5194/acp-26-3467-2026-supplement.

Author contributions. YG, CY and YL esigned the study and wrote the paper. CL, CD, YZha, YZho, XC, WM, NS, ZL, CH, XF, FZ, ZF, ZW, and YZ conducted the measurement and collected the data. HZ and YJ did the modelling. JJ, BZ and MK are acknowledged for valuable suggestions. And co-authors have read and commented on the paper.

Competing interests. The contact author has declared that none of the authors has any competing interests.

Disclaimer. Publisher's note: Copernicus Publications remains neutral with regard to jurisdictional claims made in the text, published maps, institutional affiliations, or any other geographical representation in this paper. The authors bear the ultimate responsibility for providing appropriate place names. Views expressed in the text are those of the authors and do not necessarily reflect the views of the publisher.

Acknowledgements. Heikki Junninen is acknowledged for providing the tofTool package used for processing LTOF-CIMS data.

Financial support. This research has been supported by the National Natural Science Foundation of China (NSFC) (grant no. 22327806), the Science and Technology Project of Hebei Education Department (grant no. QN2025049), and the Doctoral Fund of Hebei Vocational University of Industry and Technology (grant no. bz202402).

Review statement. This paper was edited by Dara Salcedo and reviewed by Dongjie Shang, Jie Zhang, and one anonymous referee.

References

Aalto, P., Hämeri, K., Becker, E., Weber, R., Salm, J., Mäkelä, J. M., Hoell, C., O'dowd, C. D., Hansson, H.-C., Väkevä, M., Koponen, I. K., Buzorius, G., and Kulmala, M.: Physical characterization of aerosol particles during nucleation events, Tellus B, 53, 344–358, https://doi.org/10.3402/tellusb.v53i4.17127, 2001.

Almeida, J., Schobesberger, S., Kuerten, A., Ortega, I. K., Kupiainen-Maatta, O., Praplan, A. P., Adamov, A., Amorim, A., Bianchi, F., Breitenlechner, M., David, A., Dommen, J., Donahue, N. M., Downard, A., Dunne, E., Duplissy, J., Ehrhart, S., Flagan, R. C., Franchin, A., Guida, R., Hakala, J., Hansel, A., Heinritzi, M., Henschel, H., Jokinen, T., Junninen, H., Kajos, M., Kangasluoma, J., Keskinen, H., Kupc, A., Kurten, T., Kvashin, A. N., Laaksonen, A., Lehtipalo, K., Leiminger, M., Leppa, J., Loukonen, V., Makhmutov, V., Mathot, S., McGrath, M. J., Nieminen, T., Olenius, T., Onnela, A., Petaja, T., Riccobono, F., Riipinen, I., Rissanen, M., Rondo, L., Ruuskanen, T., Santos, F. D., Sarnela, N., Schallhart, S., Schnitzhofer, R., Seinfeld, J. H., Simon, M., Sipila, M., Stozhkov, Y., Stratmann, F., Tome, A., Troestl, J., Tsagkogeorgas, G., Vaattovaara, P., Viisanen, Y., Virtanen, A., Vrtala, A., Wagner, P. E., Weingartner, E., Wex, H.,

Williamson, C., Wimmer, D., Ye, P., Yli-Juuti, T., Carslaw, K. S., Kulmala, M., Curtius, J., Baltensperger, U., Worsnop, D. R., Vehkamaki, H., and Kirkby, J.: Molecular understanding of sulphuric acid-amine particle nucleation in the atmosphere, Nature, 502, 359–363, https://doi.org/10.1038/nature12663, 2013.

Atkinson, R., Baulch, D. L., Cox, R. A., Crowley, J. N., Hampson, R. F., Hynes, R. G., Jenkin, M. E., Rossi, M. J., and Troe, J.: Evaluated kinetic and photochemical data for atmospheric chemistry: Volume I – gas phase reactions of O_x, HO_x, NO_x and SO_x species, Atmos. Chem. Phys., 4, 1461–1738, https://doi.org/10.5194/acp-4-1461-2004, 2004.

Berresheim, H., Eisele, F. L., Tanner, D. J., McInnes, L. M., Ramsey-Bell, D. C., and Covert, D. S.: Atmospheric sulfur chemistry and cloud condensation nuclei (CCN) concentrations over the northeastern Pacific Coast, J. Geophys. Res.-Atmos., 98, 12701–12711, https://doi.org/10.1029/93JD00815, 1993.

Berresheim, H., Elste, T., Plass-Dülmer, C., Eiseleb, F. L., and Tannerb, D. J.: Chemical ionization mass spectrometer for long-term measurements of atmospheric OH and H_2SO_4, Int. J. Mass Spectrom., 202, 91–109, https://doi.org/10.1016/S1387-3806(00)00233-5, 2000.

Berresheim, H., Elste, T., Tremmel, H. G., Allen, A. G., Hansson, H. C., Rosman, K., Dal Maso, M., Mäkelä, J. M., Kulmala, M., and O'Dowd, C. D.: Gas-aerosol relationships of H_2SO_4, MSA, and OH: Observations in the coastal marine boundary layer at Mace Head, Ireland, J. Geophys. Res.-Atmos., 107, PAR 5-1–PAR 5-12, https://doi.org/10.1029/2000JD000229, 2002.

Birmili, W., Berresheim, H., Plass-Dulmer, C., Elste, T., Gilge, S., Wiedensohler, A., and Uhrner, U.: The Hohenpeissenberg aerosol formation experiment (HAFEX): A long-term study including size-resolved aerosol, H_2SO_4, OH, and monoterpenes measurements, Atmos. Chem. Phys., 3, 361–376, https://doi.org/10.5194/acp-3-361-2003, 2003.

Boy, M., Karl, T., Turnipseed, A., Mauldin, R. L., Kosciuch, E., Greenberg, J., Rathbone, J., Smith, J., Held, A., Barsanti, K., Wehner, B., Bauer, S., Wiedensohler, A., Bonn, B., Kulmala, M., and Guenther, A.: New particle formation in the front range of the colorado rocky mountains, Atmos. Chem. Phys., 8, 1577–1590, https://doi.org/10.5194/acp-8-1577-2008, 2008.

Chang, X., Zheng, H., Zhao, B., Yan, C., Jiang, Y., Hu, R., Song, S., Dong, Z., Li, S., Li, Z., Zhu, Y., Shi, H., Jiang, Z., Xing, J., and Wang, S.: Drivers of High Concentrations of Secondary Organic Aerosols in Northern China during the COVID-19 Lockdowns, Environ. Sci. Technol., 57, 5521–5531, https://doi.org/10.1021/acs.est.2c06914, 2023.

Chu, B., Kerminen, V. M., Bianchi, F., Yan, C., Petäjä, T., and Kulmala, M.: Atmospheric new particle formation in China, Atmos. Chem. Phys., 19, 115–138, https://doi.org/10.5194/acp-19-115-2019, 2019.

Dada, L., Paasonen, P., Nieminen, T., Buenrostro Mazon, S., Kontkanen, J., Peräkylä, O., Lehtipalo, K., Hussein, T., Petäjä, T., Kerminen, V. M., Bäck, J., and Kulmala, M.: Long-term analysis of clear-sky new particle formation events and nonevents in Hyytiälä, Atmos. Chem. Phys., 17, 6227–6241, https://doi.org/10.5194/acp-17-6227-2017, 2017.

Dada, L., Ylivinkka, I., Baalbaki, R., Li, C., Guo, Y., Yan, C., Yao, L., Sarnela, N., Jokinen, T., Daellenbach, K. R., Yin, R., Deng, C., Chu, B., Nieminen, T., Kontkanen, J., Stolzenburg, D., Sipilä, M., Hussein, T., Paasonen, P., Bianchi, F., Salma, I., Weidinger, T., Pikridas, M., Sciare, J., Jiang, J., Liu, Y., Petäjä, T., Kerminen, V. M., and Kulmala, M.: Sources and sinks driving sulphuric acid concentrations in contrasting environments: Implications on proxy calculations, Atmos. Chem. Phys., 20, 11747–11766, https://doi.org/10.5194/acp-20-11747-2020, 2020.

Dal Maso, M., Kulmala, M., Riipinen, I., and Wagner, R.: Formation and growth of fresh atmospheric aerosols: Eight years of aerosol size distribution data from SMEAR II, Hyytiälä, Finland, Boreal Environ. Res., 10, 323–336, 2005.

Deng, C., Fu, Y., Dada, L., Yan, C., Cai, R., Yang, D., Zhou, Y., Yin, R., Lu, Y., Li, X., Qiao, X., Fan, X., Nie, W., Kontkanen, J., Kangasluoma, J., Chu, B., Ding, A., Kerminen, V.-M., Paasonen, P., Worsnop, D. R., Bianchi, F., Liu, Y., Zheng, J., Wang, L., Kulmala, M., and Jiang, J.: Seasonal characteristics of new particle formation and growth in urban Beijing, Environ. Sci. Technol., 54, 8547–8557, https://doi.org/10.1021/acs.est.0c00808, 2020.

Erupe, M. E., Benson, D. R., Li, J., Young, L.-H., Verheggen, B., Al-Refai, M., Tahboub, O., Cunningham, V., Frimpong, F., Viggiano, A. A., and Lee, S.-H.: Correlation of aerosol nucleation rate with sulfuric acid and ammonia in Kent, Ohio: An atmospheric observation, J. Geophys. Res.- Atmos., 115, D23216, https://doi.org/10.1029/2010jd013942, 2010.

Fiedler, V., Dal Maso, M., Boy, M., Aufmhoff, H., Hoffmann, J., Schuck, T., Birmili, W., Hanke, M., Uecker, J., Arnold, F., and Kulmala, M.: The contribution of sulphuric acid to atmospheric particle formation and growth: A comparison between boundary layers in Northern and Central Europe, Atmos. Chem. Phys., 5, 1773–1785, https://doi.org/10.5194/acp-5-1773-2005, 2005.

Finlayson-Pitts, B. J. and Pitts Jr., J. N.: Chemistry of the Upper and Lower Atmosphere: Theory, Experiments, and Applications, Academic Press, San Diego, CA, USA, 298–299, ISBN 9780122570605, 2000.

Gordon, H., Kirkby, J., Baltensperger, U., Bianchi, F., Breitenlechner, M., Curtius, J., Dias, A., Dommen, J., Donahue, N. M., Dunne, E. M., Duplissy, J., Ehrhart, S., Flagan, R. C., Frege, C., Fuchs, C., Hansel, A., Hoyle, C. R., Kulmala, M., Kürten, A., Lehtipalo, K., Makhmutov, V., Molteni, U., Rissanen, M. P., Stozkhov, Y., Tröstl, J., Tsagkogeorgas, G., Wagner, R., Williamson, C., Wimmer, D., Winkler, P. M., Yan, C., and Carslaw, K. S.: Causes and importance of new particle formation in the present-day and preindustrial atmospheres, J. Geophys. Res.-Atmos., 122, 8739–8760, https://doi.org/10.1002/2017JD026844, 2017.

Guo, Y., Yan, C., Li, C., Ma, W., Feng, Z., Zhou, Y., Lin, Z., Dada, L., Stolzenburg, D., Yin, R., Kontkanen, J., Daellenbach, K. R., Kangasluoma, J., Yao, L., Chu, B., Wang, Y., Cai, R., Bianchi, F., Liu, Y., and Kulmala, M.: Formation of nighttime sulfuric acid from the ozonolysis of alkenes in Beijing, Atmos. Chem. Phys., 21, 5499–5511, https://doi.org/10.5194/acp-21-5499-2021, 2021.

Guo, Y., Yan, C., Li, C., Deng, C., Zhang, Y., Zhou, Y., Zheng, H., Jiang, Y., Chen, X., Ma, W., Sarnela, N., Lin, Z., Hua, C., Fan, X., Zheng, F., Feng, Z., Wang, Z., Zhang, Y., Jiang, J., Zhao, B., Kulmala, M., and Liu Y.: Datasets for the ACP Manuscript – Measurement report: Three-year characteristics of sulfuric acid in urban Beijing and derivation of daytime sulfuric acid proxies applicable to inland sites, Zenodo [data set], https://doi.org/10.5281/zenodo.17216660, 2025.

Hartmann, C. L. A. D. L., Tank, A. M. G. K., Rusticucci, M., and Alexander, L. V.: Climate Change 2013, in: The Physical Science Basis, Working Group I Contribution to the Fifth Assessment Report of the Intergovernmental Panel on Climate Change, WMO/UNEP, Cambridge, ISBN 978-1-107-05799-9, 2014.

Jokinen, T., Sipilä, M., Junninen, H., Ehn, M., Lönn, G., Hakala, J., Petäjä, T., Mauldin III, R. L., Kulmala, M., and Worsnop, D. R.: Atmospheric sulphuric acid and neutral cluster measurements using CI-APi-TOF, Atmos. Chem. Phys., 12, 4117–4125, https://doi.org/10.5194/acp-12-4117-2012, 2012.

Jokinen, T., Sipila, M., Kontkanen, J., Vakkari, V., Tisler, P., Duplissy, E. M., Junninen, H., Kangasluoma, J., Manninen, H. E., Petaja, T., Kulmala, M., Worsnop, D. R., Kirkby, J., Virkkula, A., and Kerminen, V. M.: Ion-induced sulfuric acid-ammonia nucleation drives particle formation in coastal Antarctica, Sci. Adv., 4, eaat9744, https://doi.org/10.1126/sciadv.aat9744, 2018.

Kirkby, J., Curtius, J., Almeida, J., Dunne, E., Duplissy, J., Ehrhart, S., Franchin, A., Gagne, S., Ickes, L., Kuerten, A., Kupc, A., Metzger, A., Riccobono, F., Rondo, L., Schobesberger, S., Tsagkogeorgas, G., Wimmer, D., Amorim, A., Bianchi, F., Breitenlechner, M., David, A., Dommen, J., Downard, A., Ehn, M., Flagan, R. C., Haider, S., Hansel, A., Hauser, D., Jud, W., Junninen, H., Kreissl, F., Kvashin, A., Laaksonen, A., Lehtipalo, K., Lima, J., Lovejoy, E. R., Makhmutov, V., Mathot, S., Mikkila, J., Minginette, P., Mogo, S., Nieminen, T., Onnela, A., Pereira, P., Petaja, T., Schnitzhofer, R., Seinfeld, J. H., Sipila, M., Stozhkov, Y., Stratmann, F., Tome, A., Vanhanen, J., Viisanen, Y., Vrtala, A., Wagner, P. E., Walther, H., Weingartner, E., Wex, H., Winkler, P. M., Carslaw, K. S., Worsnop, D. R., Baltensperger, U., and Kulmala, M.: Role of sulphuric acid, ammonia and galactic cosmic rays in atmospheric aerosol nucleation, Nature, 476, 429–433, https://doi.org/10.1038/nature10343, 2011.

Kulmala, M., Lehtinen, K. E. J., and Laaksonen, A.: Cluster activation theory as an explanation of the linear dependence between formation rate of 3 nm particles and sulphuric acid concentration, Atmos. Chem. Phys., 6, 787–793, https://doi.org/10.5194/acp-6-787-2006, 2006.

Kulmala, M., Riipinen, I., Sipilä, M., Manninen, H. E., Petäjä, T., Junninen, H., Maso, M. D., Mordas, G., Mirme, A., Vana, M., Hirsikko, A., Laakso, L., Harrison, R. M., Hanson, I., Leung, C., Lehtinen, K. E. J., and Kerminen, V.-M.: Toward Direct Measurement of Atmospheric Nucleation, Science, 318, 89–92, https://doi.org/10.1126/science.1144124, 2007.

Kulmala, M., Petäjä, T., Nieminen, T., Sipilä, M., Manninen, H. E., Lehtipalo, K., Dal Maso, M., Aalto, P. P., Junninen, H., Paasonen, P., Riipinen, I., Lehtinen, K. E. J., Laaksonen, A., and Kerminen, V.-M.: Measurement of the nucleation of atmospheric aerosol particles, Nat. Protocols, 7, 1651–1667, https://doi.org/10.1038/nprot.2012.091, 2012.

Kulmala, M., Kontkanen, J., Junninen, H., Lehtipalo, K., Manninen, H. E., Nieminen, T., Petäjä, T., Sipilä, M., Schobesberger, S., Rantala, P., Franchin, A., Jokinen, T., Järvinen, E., Äijälä, M., Kangasluoma, J., Hakala, J., Aalto, P. P., Paasonen, P., Mikkilä, J., Vanhanen, J., Aalto, J., Hakola, H., Makkonen, U., Ruuskanen, T., Mauldin, R. L., Duplissy, J., Vehkamäki, H., Bäck, J., Kortelainen, A., Riipinen, I., Kurtén, T., Johnston, M. V., Smith, J. N., Ehn, M., Mentel, T. F., Lehtinen, K. E. J., Laaksonen, A., Kerminen, V.-M., and Worsnop, D. R.: Direct observations of atmospheric aerosol nucleation, Science, 339, 943–946, https://doi.org/10.1126/science.1227385, 2013.

Kürten, A., Rondo, L., Ehrhart, S., and Curtius, J.: Calibration of a Chemical Ionization Mass Spectrometer for the measurement of gaseous sulfuric acid, J. Phys. Chem. A, 116, 6375–6386, https://doi.org/10.1021/jp212123n, 2012.

Kürten, A., Jokinen, T., Simon, M., Sipila, M., Sarnela, N., Junninen, H., Adamov, A., Almeida, J., Amorim, A., Bianchi, F., Breitenlechner, M., Dommen, J., Donahue, N. M., Duplissy, J., Ehrhart, S., Flagan, R. C., Franchin, A., Hakala, J., Hansel, A., Heinritzi, M., Hutterli, M., Kangasluoma, J., Kirkby, J., Laaksonen, A., Lehtipalo, K., Leiminger, M., Makhmutov, V., Mathot, S., Onnela, A., Petaja, T., Praplan, A. P., Riccobono, F., Rissanen, M. P., Rondo, L., Schobesberger, S., Seinfeld, J. H., Steiner, G., Tome, A., Troestl, J., Winkler, P. M., Williamson, C., Wimmer, D., Ye, P., Baltensperger, U., Carslaw, K. S., Kulmala, M., Worsnop, D. R., and Curtius, J.: Neutral molecular cluster formation of sulfuric acid-dimethylamine observed in real time under atmospheric conditions, P. Natl. Acad. Sci. USA, 111, 15019–15024, https://doi.org/10.1073/pnas.1404853111, 2014.

Kürten, A., Bergen, A., Heinritzi, M., Leiminger, M., Lorenz, V., Piel, F., Simon, M., Sitals, R., Wagner, A. C., and Curtius, J.: Observation of new particle formation and measurement of sulfuric acid, ammonia, amines and highly oxidized organic molecules at a rural site in central Germany, Atmos. Chem. Phys., 16, 12793–12813, https://doi.org/10.5194/acp-16-12793-2016, 2016.

Lee, S. H., Gordon, H., Yu, H., Lehtipalo, K., Haley, R., Li, Y. X., and Zhang, R. Y.: New particle formation in the atmosphere: from molecular clusters to global climate, J. Geophys. Res.-Atmos., 124, 7098–7146, https://doi.org/10.1029/2018jd029356, 2019.

Lehtipalo, K., Yan, C., Dada, L., Bianchi, F., Xiao, M., Wagner, R., Stolzenburg, D., Ahonen, L., Amorim, A., Baccarini, A., Bauer, P., Baumgartner, B., Bergen, A., Bernhammer, A.-K., Breitenlechner, M., Brilke, S., Buchholz, A., Mazon, S., Chen, D., and Worsnop, D.: Multicomponent new particle formation from sulfuric acid, ammonia, and biogenic vapors, Sci. Adv., 4, eaau5363, https://doi.org/10.1126/sciadv.aau5363, 2018.

Lelieveld, J., Evans, J. S., Fnais, M., Giannadaki, D., and Pozzer, A.: The contribution of outdoor air pollution sources to premature mortality on a global scale, Nature, 525, 367–371, https://doi.org/10.1038/nature15371, 2015.

Liu, J., Jiang, J., Zhang, Q., Deng, J., and Hao, J.: A spectrometer for measuring particle size distributions in the range of 3 nm to 10 µm, Front. Environ. Sci. Eng., 10, 63–72, https://doi.org/10.1007/s11783-014-0754-x, 2016.

Liu, Y., Yan, C., Feng, Z., Zheng, F., Fan, X., Zhang, Y., Li, C., Zhou, Y., Lin, Z., Guo, Y., Zhang, Y., Ma, L., Zhou, W., Liu, Z., Dada, L., Dällenbach, K., Kontkanen, J., Cai, R., Chan, T., Chu, B., Du, W., Yao, L., Wang, Y., Cai, J., Kangasluoma, J., Kokkonen, T., Kujansuu, J., Rusanen, A., Deng, C., Fu, Y., Yin, R., Li, X., Lu, Y., Liu, Y., Lian, C., Yang, D., Wang, W., Ge, M., Wang, Y., Worsnop, D. R., Junninen, H., He, H., Kerminen, V.-M., Zheng, J., Wang, L., Jiang, J., Petäjä, T., Bianchi, F., and Kulmala, M.: Continuous and comprehensive atmospheric observations in Beijing: A station to understand the complex urban atmospheric environment, Big Earth Data, 4, 295–321, https://doi.org/10.1080/20964471.2020.1798707, 2020.

Lu, K. D., Rohrer, F., Holland, F., Fuchs, H., Bohn, B., Brauers, T., Chang, C. C., Häseler, R., Hu, M., Kita, K., Kondo, Y., Li, X., Lou, S. R., Nehr, S., Shao, M., Zeng, L. M., Wahner, A., Zhang, Y. H., and Hofzumahaus, A.: Observation and modelling of OH and HO_2 concentrations in the Pearl River Delta 2006: A missing OH source in a VOC rich atmosphere, Atmos. Chem. Phys., 12, 1541–1569, https://doi.org/10.5194/acp-12-1541-2012, 2012.

Lu, Y., Yan, C., Fu, Y., Chen, Y., Liu, Y., Yang, G., Wang, Y., Bianchi, F., Chu, B., Zhou, Y., Yin, R., Baalbaki, R., Garmash, O., Deng, C., Wang, W., Liu, Y., Petaja, T., Kerminen, V.-M., Jiang, J., Kulmala, M., and Wang, L.: A proxy for atmospheric daytime gaseous sulfuric acid concentration in urban Beijing, Atmos. Chem. Phys., 19, 1971–1983, https://doi.org/10.5194/acp-19-1971-2019, 2019.

Ma, L., Zhu, Y., Zheng, M., Sun, Y., Huang, L., Liu, X., Gao, Y., Shen, Y., Gao, H., and Yao, X.: Investigating three patterns of new particles growing to the size of cloud condensation nuclei in Beijing's urban atmosphere, Atmos. Chem. Phys., 21, 183–200, https://doi.org/10.5194/acp-21-183-2021, 2021.

Ma, X., Tan, Z., Lu, K., Yang, X., Liu, Y., Li, S., Li, X., Chen, S., Novelli, A., Cho, C., Zeng, L., Wahner, A., and Zhang, Y.: Winter photochemistry in Beijing: Observation and model simulation of OH and HO_2 radicals at an urban site, Sci. Total Environ., 685, 85–95, https://doi.org/10.1016/j.scitotenv.2019.05.329, 2019.

Ma, X., Tan, Z., Lu, K., Yang, X., Chen, X., Wang, H., Chen, S., Fang, X., Li, S., Li, X., Liu, J., Liu, Y., Lou, S., Qiu, W., Wang, H., Zeng, L., and Zhang, Y.: OH and HO_2 radical chemistry at a suburban site during the EXPLORE-YRD campaign in 2018, Atmos. Chem. Phys., 22, 7005–7028, https://doi.org/10.5194/acp-22-7005-2022, 2022.

Manninen, H. E., Nieminen, T., Riipinen, I., Yli-Juuti, T., Gagné, S., Asmi, E., Aalto, P. P., Petäjä, T., Kerminen, V. M., and Kulmala, M.: Charged and total particle formation and growth rates during EUCAARI 2007 campaign in Hyytiälä, Atmos. Chem. Phys., 9, 4077–4089, https://doi.org/10.5194/acp-9-4077-2009, 2009.

Mauldin, R. L., Eisele, F. L., Tanner, D. J., Kosciuch, E., Shetter, R., Lefer, B., Hall, S. R., Nowak, J. B., Buhr, M., Chen, G., Wang, P., and Davis, D.: Measurements of OH, H_2SO_4, and MSA at the South Pole during ISCAT, Geophys. Res. Lett., 28, 3629–3632, https://doi.org/10.1029/2000gl012711, 2001.

Mauldin, R. L., Kosciuch, E., Henry, B., Eisele, F. L., Shetter, R., Lefer, B., Chen, G., Davis, D., Huey, G., and Tanner, D.: Measurements of OH, HO_2+RO_2, H_2SO_4, and MSA at the South Pole during ISCAT 2000, Atmos. Environ., 38, 5423–5437, https://doi.org/10.1016/j.atmosenv.2004.06.031, 2004.

McMurry, P. H., Fink, M., Sakurai, H., Stolzenburg, M. R., Mauldin, R. L., Smith, J., Eisele, F., Moore, K., Sjostedt, S., Tanner, D., Huey, L. G., Nowak, J. B., Edgerton, E., and Voisin, D.: A criterion for new particle formation in the sulfur-rich Atlanta atmosphere, J. Geophys. Res.-Atmos., 110, D22S02, https://doi.org/10.1029/2005jd005901, 2005.

Merikanto, J., Spracklen, D. V., Mann, G. W., Pickering, S. J., and Carslaw, K. S.: Impact of nucleation on global CCN, Atmos. Chem. Phys., 9, 8601–8616, https://doi.org/10.5194/acp-9-8601-2009, 2009.

Mikkonen, S., Romakkaniemi, S., Smith, J. N., Korhonen, H., Petäjä, T., Plass-Duelmer, C., Boy, M., McMurry, P. H., Lehtinen, K. E. J., Joutsensaari, J., Hamed, A., Mauldin Iii, R. L., Birmili, W., Spindler, G., Arnold, F., Kulmala, M., and Laaksonen, A.: A statistical proxy for sulphuric acid concentration, Atmos. Chem. Phys., 11, 11319–11334, https://doi.org/10.5194/acp-11-11319-2011, 2011.

Myllys, N., Chee, S., Olenius, T., Lawler, M., and Smith, J.: Molecular-level understanding of synergistic effects in sulfuric acid-amine-ammonia mixed clusters, J. Phys. Chem. A, 123, 2420–2425, https://doi.org/10.1021/acs.jpca.9b00909, 2019.

Nieminen, T., Manninen, H. E., Sihto, S. L., Yli-Juuti, T., Mauldin, I. R. L., Petäjä, T., Riipinen, I., Kerminen, V. M., and Kulmala, M.: Connection of sulfuric acid to atmospheric nucleation in boreal forest, Environ. Sci. Technol., 43, 4715–4721, https://doi.org/10.1021/es803152j, 2009.

Nieminen, T., Kerminen, V. M., Petäjä, T., Aalto, P. P., Arshinov, M., Asmi, E., Baltensperger, U., Beddows, D. C. S., Beukes, J. P., Collins, D., Ding, A., Harrison, R. M., Henzing, B., Hooda, R., Hu, M., Hõrrak, U., Kivekäs, N., Komsaare, K., Krejci, R., Kristensson, A., Laakso, L., Laaksonen, A., Leaitch, W. R., Lihavainen, H., Mihalopoulos, N., Németh, Z., Nie, W., O'Dowd, C., Salma, I., Sellegri, K., Svenningsson, B., Swietlicki, E., Tunved, P., Ulevicius, V., Vakkari, V., Vana, M., Wiedensohler, A., Wu, Z., Virtanen, A., and Kulmala, M.: Global analysis of continental boundary layer new particle formation based on long-term measurements, Atmos. Chem. Phys., 18, 14737–14756, https://doi.org/10.5194/acp-18-14737-2018, 2018.

O'Dowd, C. D., Aalto, P., Hmeri, K., Kulmala, M., and Hoffmann, T.: Atmospheric particles from organic vapours, Nature, 416, 497–498, https://doi.org/10.1038/416497a, 2002.

Paasonen, P., Sihto, S.-L., Nieminen, T., Vuollekoski, H., Riipinen, I., Plass-Dulmer, C., Berresheim, H., Birmili, W., and Kulmala, M.: Connection between new particle formation and sulphuric acid at Hohenpeissenberg (Germany) including the influence of organic compounds, Boreal Environ. Res., 14, 616–629, 2009.

Petäjä, T., Mauldin, I. R. L., Kosciuch, E., McGrath, J., Nieminen, T., Paasonen, P., Boy, M., Adamov, A., Kotiaho, T., and Kulmala, M.: Sulfuric acid and OH concentrations in a boreal forest site, Atmos. Chem. Phys., 9, 7435–7448, https://doi.org/10.5194/acp-9-7435-2009, 2009.

Qi, X. M., Ding, A. J., Nie, W., Petäjä, T., Kerminen, V. M., Herrmann, E., Xie, Y. N., Zheng, L. F., Manninen, H., Aalto, P., Sun, J. N., Xu, Z. N., Chi, X. G., Huang, X., Boy, M., Virkkula, A., Yang, X. Q., Fu, C. B., and Kulmala, M.: Aerosol size distribution and new particle formation in the western Yangtze River Delta of China: 2 years of measurements at the SORPES station, Atmos. Chem. Phys., 15, 12445–12464, https://doi.org/10.5194/acp-15-12445-2015, 2015.

Riccobono, F., Schobesberger, S., Scott, C., Dommen, J., Ortega, I., Rondo, L., Almeida, J., Amorim, A., Bianchi, F., Breitenlechner, M., David, A., Downard, A., Dunne, E., Duplissy, J., Ehrhart, S., Flagan, R., Franchin, A., Hansel, A., Junninen, H., and Baltensperger, U.: Oxidation products of biogenic emissions contribute to nucleation of atmospheric particles, Science, 344, 717–721, https://doi.org/10.1126/science.1243527, 2014.

Riipinen, I., Sihto, S. L., Kulmala, M., Arnold, F., Dal Maso, M., Birmili, W., Saarnio, K., Teinila, K., Kerminen, V. M., Laaksonen, A., and Lehtinen, K. E. J.: Connections between atmospheric sulphuric acid and new particle formation during QUEST III–IV campaigns in Heidelberg and Hyytiälä, Atmos. Chem. Phys., 7, 1899–1914, https://doi.org/10.5194/acp-7-1899-2007, 2007.

Rohrer, F. and Berresheim, H.: Strong correlation between levels of tropospheric hydroxyl radicals and solar ultraviolet radiation, Nature, 442, 184–187, https://doi.org/10.1038/nature04924, 2006.

Sarnela, N., Jokinen, T., Nieminen, T., Lehtipalo, K., Junninen, H., Kangasluoma, J., Hakala, J., Taipale, R., Schobesberger, S., Sipila, M., Larnimaa, K., Westerholm, H., Heijari, J., Kerminen, V.-M., Petaja, T., and Kulmala, M.: Sulphuric acid and aerosol particle production in the vicinity of an oil refinery, Atmos. Environ., 119, 156–166, https://doi.org/10.1016/j.atmosenv.2015.08.033, 2015.

Sarwar, G., Appel, K. W., Carlton, A. G., Mathur, R., Schere, K., Zhang, R., and Majeed, M. A.: Impact of a new condensed toluene mechanism on air quality model predictions in the US, Geosci. Model Dev., 4, 183–193, https://doi.org/10.5194/gmd-4-183-2011, 2011.

Tan, Z., Fuchs, H., Lu, K., Hofzumahaus, A., Bohn, B., Broch, S., Dong, H., Gomm, S., Häseler, R., He, L., Holland, F., Li, X., Liu, Y., Lu, S., Rohrer, F., Shao, M., Wang, B., Wang, M., Wu, Y., Zeng, L., Zhang, Y., Wahner, A., and Zhang, Y.: Radical chemistry at a rural site (Wangdu) in the North China Plain: Observation and model calculations of OH, HO_2 and RO_2 radicals, Atmos. Chem. Phys., 17, 663–690, https://doi.org/10.5194/acp-17-663-2017, 2017.

Tan, Z., Rohrer, F., Lu, K., Ma, X., Bohn, B., Broch, S., Dong, H., Fuchs, H., Gkatzelis, G. I., Hofzumahaus, A., Holland, F., Li, X., Liu, Y., Liu, Y., Novelli, A., Shao, M., Wang, H., Wu, Y., Zeng, L., Hu, M., Kiendler-Scharr, A., Wahner, A., and Zhang, Y.: Wintertime photochemistry in Beijing: Observations of RO_x radical concentrations in the North China Plain during the BEST-ONE campaign, Atmos. Chem. Phys., 18, 12391–12411, https://doi.org/10.5194/acp-18-12391-2018, 2018.

Wang, Z. B., Hu, M., Yue, D. L., Zheng, J., Zhang, R. Y., Wiedensohler, A., Wu, Z. J., Nieminen, T., and Boy, M.: Evaluation on the role of sulfuric acid in the mechanisms of new particle formation for Beijing case, Atmos. Chem. Phys., 11, 12663–12671, https://doi.org/10.5194/acp-11-12663-2011, 2011.

Weber, R. J., McMurry, P. H., Eisele, F. L., and Tanner, D. J.: Measurement of expected nucleation precursor species and 3–500-nm diameter particles at Mauna Loa observatory, Hawaii, J. Atmos. Sci., 52, 2242–2257, https://doi.org/10.1175/1520-0469(1995)052<2242:MOENPS>2.0.CO;2, 1995.

Weber, R. J., Marti, J. J., McMurry, P. H., Eisele, F. L., Tanner, D. J., and Jefferson, A.: Measured atmospheric new particle formation rates: Implications for nucleation mechanisms, Chem. Eng. Commun., 151, 53–64, 1996.

Weber, R. J., Marti, J. J., McMurry, P. H., Eisele, F. L., Tanner, D. J., and Jefferson, A.: Measurements of new particle formation and ultrafine particle growth rates at a clean continental site, J. Geophys. Res.-Atmos., 102, 4375–4385, https://doi.org/10.1029/96jd03656, 1997.

Weber, R. J., McMurry, P. H., Mauldin, L., Tanner, D. J., Eisele, F. L., Brechtel, F. J., Kreidenweis, S. M., Kok, G. L., Schillawski, R. D., and Baumgardner, D.: A study of new particle formation and growth involving biogenic and trace gas species measured during ACE 1, J. Geophys. Res.-Atmos., 103, 16385–16396, https://doi.org/10.1029/97jd02465, 1998.

Wine, P. H., Thompson, R. J., Ravishankara, A. R., Semmes, D. H., Gump, C. A., Torabi, A., and Nicovich, J. M.: Kinetics of the reaction $OH + SO_2 + M \rightarrow HOSO_2 + M$: Temperature and pressure dependence in the fall-off region, J. Phys. Chem., 88, 2104–2109, 1984.

Yan, C., Yin, R., Lu, Y., Dada, L., Yang, D., Fu, Y., Kontkanen, J., Deng, C., Garmash, O., Ruan, J., Baalbaki, R., Schervish, M., Cai, R., Bloss, M., Chan, T., Chen, T., Chen, Q., Chen, X., Chen, Y., Chu, B., Dällenbach, K., Foreback, B., He, X., Heikkinen, L., Jokinen, T., Junninen, H., Kangasluoma, J., Kokkonen, T., Kurppa, M., Lehtipalo, K., Li, H., Li, H., Li, X., Liu, Y., Ma, Q., Paasonen, P., Rantala, P., Pileci, R. E., Rusanen, A., Sarnela, N., Simonen, P., Wang, S., Wang, W., Wang, Y., Xue, M., Yang, G., Yao, L., Zhou, Y., Kujansuu, J., Petäjä, T., Nie, W., Ma, Y., Ge, M., He, H., Donahue, N. M., Worsnop, D. R., Veli-Matti, K., Wang, L., Liu, Y., Zheng, J., Kulmala, M., Jiang, J., and Bianchi, F.: The synergistic role of sulfuric acid, bases, and oxidized organics governing new-particle formation in Beijing, Geophys. Res. Lett., 48, e2020GL091944, https://doi.org/10.1029/2020GL091944, 2021.

Yan, C., Shen, Y., Stolzenburg, D., Dada, L., Qi, X., Hakala, S., Sundström, A.-M., Guo, Y., Lipponen, A., Kokkonen, T. V., Kontkanen, J., Cai, R., Cai, J., Chan, T., Chen, L., Chu, B., Deng, C., Du, W., Fan, X., He, X.-C., Kangasluoma, J., Kujansuu, J., Kurppa, M., Li, C., Li, Y., Lin, Z., Liu, Y., Liu, Y., Lu, Y., Nie, W., Pulliainen, J., Qiao, X., Wang, Y., Wen, Y., Wu, Y., Yang, G., Yao, L., Yin, R., Zhang, G., Zhang, S., Zheng, F., Zhou, Y., Arola, A., Tamminen, J., Paasonen, P., Sun, Y., Wang, L., Donahue, N. M., Liu, Y., Bianchi, F., Daellenbach, K. R., Worsnop, D. R., Kerminen, V.-M., Petäjä, T., Ding, A., Jiang, J., and Kulmala, M.: The effect of COVID-19 restrictions on atmospheric new particle formation in Beijing, Atmos. Chem. Phys., 22, 12207–12220, https://doi.org/10.5194/acp-22-12207-2022, 2022.

Yang, C., Dong, H., Chen, Y., Wang, Y., Fan, X., Tham, Y. J., Chen, G., Xu, L., Lin, Z., Li, M., Hong, Y., and Chen, J.: Machine Learning Reveals the Parameters Affecting the Gaseous Sulfuric Acid Distribution in a Coastal City: Model Construction and Interpretation, Environ. Sci. Technol. Lett., 10, 1045–1051, https://doi.org/10.1021/acs.estlett.3c00170, 2023.

Yang, L., Nie, W., Liu, Y., Xu, Z., Xiao, M., Qi, X., Li, Y., Wang, R., Zou, J., Paasonen, P., Yan, C., Xu, Z., Wang, J., Zhou, C., Yuan, J., Sun, J., Chi, X., Kerminen, V.-M., Kulmala, M., and Ding, A.: Toward building a physical proxy for gas-phase sulfuric acid concentration based on its budget analysis in polluted Yangtze River Delta, East China, Environ. Sci. Technol., 55, 6665–6676, https://doi.org/10.1021/acs.est.1c00738, 2021a.

Yang, X., Lu, K., Ma, X., Liu, Y., Wang, H., Hu, R., Li, X., Lou, S., Chen, S., Dong, H., Wang, F., Wang, Y., Zhang, G., Li, S., Yang, S., Yang, Y., Kuang, C., Tan, Z., Chen, X., Qiu, P., Zeng, L., Xie, P., and Zhang, Y.: Observations and modeling of OH and HO_2 radicals in Chengdu, China in summer 2019, Sci. Total Environ., 772, 144829, https://doi.org/10.1016/j.scitotenv.2020.144829, 2021b.

Yao, L., Garmash, O., Bianchi, F., Zheng, J., Yan, C., Kontkanen, J., Junninen, H., Mazon, S. B., Ehn, M., Paasonen, P., Sipila, M., Wang, M. Y., Wang, X. K., Xiao, S., Chen, H. F., Lu, Y. Q., Zhang, B. W., Wang, D. F., Fu, Q. Y., Geng, F. H., Li, L., Wang, H. L., Qiao, L. P., Yang, X., Chen, J. M., Kerminen, V. M., Petaja, T., Worsnop, D. R., Kulmala, M., and Wang, L.: Atmospheric new particle formation from sulfuric

acid and amines in a Chinese megacity, Science, 361, 278–281, https://doi.org/10.1126/science.aao4839, 2018.

Yao, L., Fan, X., Yan, C., Kurtén, T., Daellenbach, K. R., Li, C., Wang, Y., Guo, Y., Dada, L., Rissanen, M. P., Cai, J., Tham, Y. J., Zha, Q., Zhang, S., Du, W., Yu, M., Zheng, F., Zhou, Y., Kontkanen, J., Chan, T., Shen, J., Kujansuu, J. T., Kangasluoma, J., Jiang, J., Wang, L., Worsnop, D. R., Petäjä, T., Kerminen, V.-M., Liu, Y., Chu, B., He, H., Kulmala, M., and Bianchi, F.: Unprecedented ambient sulfur trioxide (SO_3) detection: Possible formation mechanism and atmospheric implications, Environ. Sci. Technol. Lett., 7, 809–818, https://doi.org/10.1021/acs.estlett.0c00615, 2020.

Yu, H., McGraw, R., and Lee, S.-H.: Effects of amines on formation of sub-3 nm particles and their subsequent growth, Geophys. Res. Lett., 39, https://doi.org/10.1029/2011gl050099, 2012.

Zhao, B., Wang, S., Donahue, N. M., Jathar, S. H., Huang, X., Wu, W., Hao, J., and Robinson, A. L.: Quantifying the effect of organic aerosol aging and intermediate-volatility emissions on regional-scale aerosol pollution in China, Sci. Rep., 6, 28815, https://doi.org/10.1038/srep28815, 2016.

Zhao, B., Zheng, H., Wang, S., Smith, K. R., Lu, X., Aunan, K., Gu, Y., Wang, Y., Ding, D., Xing, J., Fu, X., Yang, X., Liou, K.-N., and Hao, J.: Change in household fuels dominates the decrease in $PM_{2.5}$ exposure and premature mortality in China in 2005–2015, P. Natl. Acad. Sci. USA, 115, 12401–12406, https://doi.org/10.1073/pnas.1812955115, 2018.

Zheng, H., Cai, S., Wang, S., Zhao, B., Chang, X., and Hao, J.: Development of a unit-based industrial emission inventory in the Beijing–Tianjin–Hebei region and resulting improvement in air quality modeling, Atmos. Chem. Phys., 19, 3447–3462, https://doi.org/10.5194/acp-19-3447-2019, 2019a.

Zheng, H., Zhao, B., Wang, S., Wang, T., Ding, D., Chang, X., Liu, K., Xing, J., Dong, Z., Aunan, K., Liu, T., Wu, X., Zhang, S., and Wu, Y.: Transition in source contributions of $PM_{2.5}$ exposure and associated premature mortality in China during 2005–2015, Environ. Int., 132, 105111, https://doi.org/10.1016/j.envint.2019.105111, 2019b.

Zheng, H., Song, S., Sarwar, G., Gen, M., Wang, S., Ding, D., Chang, X., Zhang, S., Xing, J., Sun, Y., Ji, D., Chan, C. K., Gao, J., and McElroy, M. B.: Contribution of Particulate Nitrate Photolysis to Heterogeneous Sulfate Formation for Winter Haze in China, Environ. Sci. Technol. Lett., 7, 632–638, https://doi.org/10.1021/acs.estlett.0c00368, 2020.

Zheng, H., Chang, X., Wang, S., Li, S., Zhao, B., Dong, Z., Ding, D., Jiang, Y., Huang, G., Huang, C., An, J., Zhou, M., Qiao, L., and Xing, J.: Sources of Organic Aerosol in China from 2005 to 2019: A Modeling Analysis, Environ. Sci. Technol., 57, 5957–5966, https://doi.org/10.1021/acs.est.2c08315, 2023.

Zheng, H., Li, S., Jiang, Y., Dong, Z., Yin, D., Zhao, B., Wu, Q., Liu, K., Zhang, S., Wu, Y., Wen, Y., Xing, J., Henneman, L. R. F., Kinney, P. L., Wang, S., and Hao, J.: Unpacking the factors contributing to changes in $PM_{2.5}$-associated mortality in China from 2013 to 2019, Environ. Int., 184, 108470, https://doi.org/10.1016/j.envint.2024.108470, 2024.

Zhou, Y., Hakala, S., Yan, C., Gao, Y., Yao, X., Chu, B., Chan, T., Kangasluoma, J., Gani, S., Kontkanen, J., Paasonen, P., Liu, Y., Petäjä, T., Kulmala, M., and Dada, L.: Measurement report: New particle formation characteristics at an urban and a mountain station in northern China, Atmos. Chem. Phys., 21, 17885–17906, https://doi.org/10.5194/acp-21-17885-2021, 2021.